Centre for Geo-Information

Thesis Report GIRS-2014-04

LIDAR based estimation of roof-top photovoltaic potential of Wageningen

Case of Wageningen Municipality

Eva Marešová

May 2014

WAGENINGEN UNIVERSITY
WAGENINGEN UR

LIDAR based estimation of roof-top photovoltaic potential of Wageningen

Eva Marešová

Registration number 881130543020

Supervisors:

Ron van Lammeren
Ingo Leusbrock

A thesis submitted in partial fulfilment of the degree of Master of Science
at Wageningen University and Research Centre,
The Netherlands.

29.4.2014
Wageningen, The Netherlands

Thesis code number: GRS-80436
Thesis Report: GIRS-2014-04
Wageningen University and Research Centre
Laboratory of Geo-Information Science and Remote Sensing

Acknowledgement

This report is the results of my MSc thesis research. During working on this thesis I gained experience with handling, visualizing and processing of LIDAR data.
First of all I would like to thank my supervisors Ron van Lammeren and Ingo Leusbrock for their periodical feedback and valuable inputs on our meetings. Further thanks to my MGI classmates for respecting my endless analysis running on several computers over the weekends and some days in a week. I would also like to thank Frédéric Back from Tetraeder.solar for his interest and e-mail communication regarding validation of this thesis. I must not forget Erwin Pier, my second reader for his useful comments and feedback. Special thanks belongs to all my housemates who made my time in Wageningen so fantastic.

Contents

List of abbreviations

ALS = Airborne laser scanning
DSM = Digital Surface Model
DTM = Digital Terrain Model
GIS = Geographic Information System
LIDAR = Light Detection and Ranging
PC = postal code
PV = photovoltaics
TIN = triangulated irregular network

Glossary

Clearness index Ratio of the global irradiance on a horizontal plane (on the earth surface) to the respective irradiance just outside of the atmosphere.

Clear-sky index Ratio of the global irradiance on a horizontal plane to the irradiance expected under clear-sky conditions.

Cold spots of solar potential are sites where solar energy potential is lower than local electricity demand

Geographic information system (GIS) is a computerized system used for analyzing various layers of data that refer to geographical locations, by merging cartography and database technology.

Global positioning system (GPS) A global navigation satellite system providing location and time information at any location with an unobstructed line of sight to at least four dedicated satellites.

Hot spots of solar potential are sites where solar energy potential is higher than local electricity demand

Electricity demand cover is a capacity per year to cover electricity consumption (percentage)

Electricity grid is an interconnected network for delivering electricity from suppliers to consumers. It consists of generating stations that produce electrical power, high-voltage transmission lines that carry power from distant sources to demand centers, and distribution lines that connect individual customers.

Insolation is the cumulative sum of all the energy that has been collected on a surface area within a given time. Insolation = Energy * Time / Area

Irradiance is the rate of energy that is being delivered to a surface area at any given time. It denotes the instantaneous rate in which power is delivered to a surface. Irradiance = Energy / Area

Mismatch is the difference between energy supply and demand

Photovoltaic cell is a small conductive device which converts visible light into electricity

Pyranometer is an instrument measuring short wave radiation (global, reflected, net)

Roof patch individual roof planes distinguished based on slope and orientation

Triangular irregular networks are digital means used in GIS to represent surface morphology

Zonatlas is a solar cadaster website where public can find solar potential of their roof and suitability for solar panel installation

Abstract

Renewable energy sources, especially electricity production via photovoltaic panels, are becoming increasingly competitive with conventional energy sources and represent a promising option for decentralized energy supply. Nevertheless, a careful evaluation of the actual location of e.g. a PV panel is still needed as efficiency and overall performance is highly influenced by the exposure to sunlight. Thus, the identification of suitable roof surfaces within cities is attracting increasing attention of planners and researchers in recent years. These systems can contribute to self-sufficiency and decrease greenhouse gases emissions in urban areas while making use of so far unused surfaces. The aim of this study is to calculate solar potential of roofs in Wageningen, their suitability for installation of photovoltaic systems, assessment of the impact of trees shading on the overall potential and uncertainty arising from different ways of roof outlines detection.

Yearly photovoltaic potential was calculated with the ESRI ArcGIS Solar Analyst tool using LIDAR, cadastral and meteorological data and LIDAR-based outlines were derived for comparison with cadaster outlines.

82% of LIDAR based footprints were in good agreement with data from the building cadaster. Assuming only 75% of all roof surfaces are usable for PV installation, 2/3 of yearly consumption of Wageningen could be covered. Tree shading has a negative effect of 21% in less vegetated areas and 43,5% in more vegetated areas in comparison to a situation without vegetation.

The outcomes of this study can be used for planning where to install PV with which priority and eventually meet the ambition of the municipality of Wageningen to become climate neutral in 2030. Based on the current results, a considerable proportion of Wageningen can be classified as self-sufficient or nearly self-sufficient on a yearly base in terms of electricity supply.

1 Introduction

1.1 Context and background

Energy consumption is rapidly increasing due to growing world population and economic development. According to International Energy Outlook 2013, the world's energy consumption is expected to grow by 56% from 2010 to 2040 (EIA, 2013). Because fossil fuels are a limited source of energy, the transition towards renewable energy sources is inevitable (Salameh, 2003). The percentage of renewable energy will increasingly contribute to the energy mix in coming years (EIA, 2013).

1.1.1 Solar energy

Since solar energy is the major non depletable source of renewable energy, technology development and increased cost-efficiency is expected to make solar energy a mainstream energy source within the next decades (see Figure 1). The installed PV capacity in the Netherlands is persistent, in 2011 compared to 2010 it increased by 25% (Bortolini, Gamberi, Graziani, Mora, & Regattieri, 2013). Currently, the global cumulative installed PV capacity is 71 GW, of which 66 GW is supplying world's electrical networks (Palz, 2012) and according to International Energy Agency, PV energy is expected to produce around 11% of the world's final energy demand by 2050 (EREC, 2011).

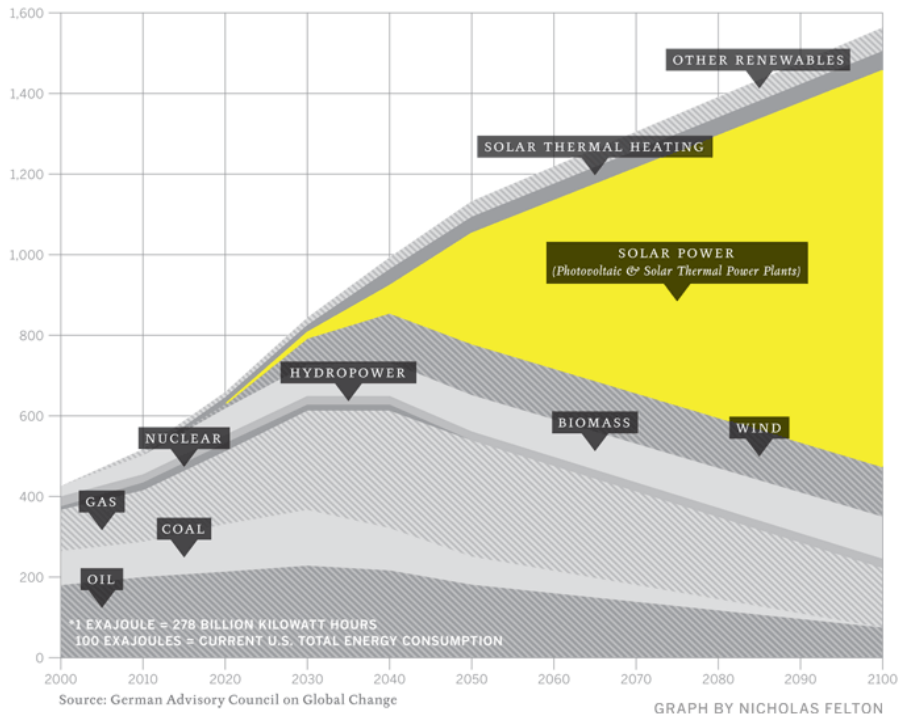

Figure 1: Projected share by source of annual global energy production (EJ/year) (WBGU, 2013)

1.1.2 Roof-top photovoltaic

Since appropriate siting of solar energy collectors is depending on energy efficiency and public acceptance (Tsoutsos, Frantzeskaki, & Gekas, 2005), building roofs represent a great potential for producing solar energy (Wittmann, Bajons, Doneus, & Friesinger, 1997). However in order to generate sufficient amounts of energy for meaningful use, large space required for concentrating PV panels is needed (van den Dobbelsteen & Stremke, 2013). The most favourable locations for PV system installation are large roof areas of commercial and industrial buildings (Thomas, Britain, Fordham, & Architects, 1999).

1.1.3 Photovoltaic Solar Cells

Solar cell, also called PV cell, is a device that can convert sunlight's photon into electricity. PV cells are usually connected in modules in order to provide a substantial electrical power. The photovoltaic technology offers the following advantages. It is a clean technology which does not produce any toxic or radioactive waste. Solar panels provide reliable energy, require low maintenance and its life span expectation is between 20 and 30 years (Ibrahim, Othman, Ruslan, Mat, & Sopian, 2011).

1.2 Airborne LIDAR technique

The 'Light Detection and Ranging' technique, or LIDAR, is a laser application of remote sensing used for measurement distances to features and the ground. It provides range data as 3D point clouds.
The laser ranging system transmits optical laser light in pulses toward the Earth's surface and measures the travel time of the transmitted and reflected pulse (see Figure 2). Based on the time of travel of the laser pulse the distance between the transmitter and reflector is determined (Flood & Gutelius, 1997; Wehr & Lohr, 1999).

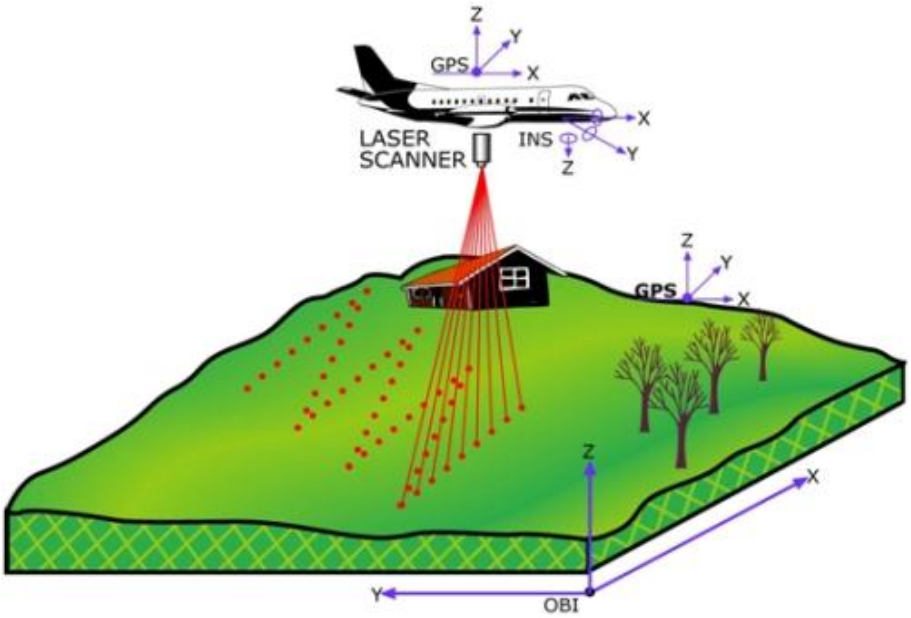

Figure 2: Principle of LIDAR scanning ("ASPRS," 2012)

LIDAR requires precise knowledge of the platform's location and orientation. Besides the laser ranging system, LIDAR consists of two GPS receivers and an inertial navigation system (INS). One GPS receiver is installed on the aircraft; the second is situated at a known ground location. Based on the location and orientation of the scanner (from the GPS and INS), the angle of the scan mirror, and the range distance to the object the x/y/z coordinate of each return is calculated. To avoid the gaps between strips, LIDAR passes numerous times at different angles (Flood & Gutelius, 1997; Wehr & Lohr, 1999).

LIDAR aerial scanning results in a collection of unstructured 3D points (point clouds). These raw LIDAR data allow the generation of digital surface models (DSM) of the ground surface. DSM depicts the topography of the earth's surface, including objects above the terrain. Digital Terrain Models (DTM) and surface object models like buildings can be derived in further processing (see Figure 3). Over the years the application of LIDAR has been extended, detected buildings provide variety of application such as urban environmental planning and design (Yu, Liu, Wu, Hu, & Zhang, 2010), disaster management (Dash, Steinle, Singh, & Bähr,

2004), virtual tourism (Georgopoulos & Tsakiri, 2004) and solar energy potential analysis (Hofierka & Kaňuk, 2009; Lukač, Žlaus, Seme, Žalik, & Štumberger, 2012).

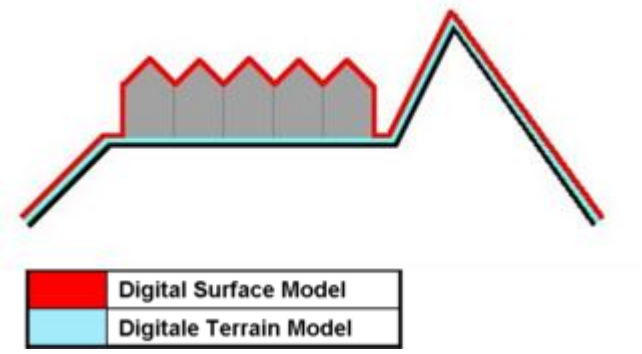

Figure 3: DSM represents surface with objects on it, DTM represents the bare ground (Wikipedia, 2013a)

1.2.1 Motivation of use of LIDAR data

LIDAR data offers height information with high degree of accuracy and short time acquisition. Unlike photogrammetry which relies on aerial images the active, LIDAR technology is less sensitive to cloud cover and shadows. Moreover cost of LIDAR data is nowadays decreasing. High geometric detail of LIDAR data enables to calculate the solar radiation of an area of interest and subsequently find suitable roof areas for PV installation. Rising availability of LIDAR data implies number of applications in environmental planning.

Problem definition

Based on climate and energy targets set by European Commission known as "20-20-20" (20% increase in energy efficiency, 20% reduction of CO_2 emissions, and 20% renewables by 2020), the municipality of Wageningen wants to reduce its environmental impact. The ambition of the municipality is to be climate neutral by 2030 (Zonne Energie Wageningen, 2012). There are several similar incentives across the Netherlands aiming to become climate neutral by preserving resources, reducing its carbon footprint and minimize the effects of energy price increases and price instability. Nevertheless according to Dutch Renewable Energy Council it is uncertain whether the Netherlands will reach its 2020 Renewable energy target with current measures (EREC, 2011).

These incentives try to promote and stimulate the use of low carbon energy resources, like PV (IEA PVPS, 2012). A precondition for the suitable location of solar panel and for the assessment of its potential is the knowledge of global solar radiation distribution for a given location. However, the yearly potential for solar electricity in the Netherlands is low and positions the Netherlands into last but one of most favorable regions within the EU (Šúri, Huld, Dunlop, & Ossenbrink, 2007). In order to support PV initiatives, solar potential of rooftop, potential energy savings, installation costs and payback times represents meaningful information. Within this context, some cities created solar potential maps, to promote renewable energy generation through PV panel installations.

While a number of cities have already created solar potential maps, limited attention has been paid to underlying assumptions. Also the methods used in related research differ. In order to obtain solar radiation intensity, roof top solar panel installations must be installed according to many parameters (e.g. optimum tilt, orientation, minimal shading effect). The potential of each available rooftop must be assessed before implementing a PV infrastructure (IEA PVPS, 2002).

The solar panels should be installed in a way to produce enough electricity to reduce or eliminate dependency on conventional energy (Orioli & Di Gangi, 2013). Proper matching of PV supply and load demand is essential. The concept of cold and hot spots describes the mismatch between energy supply and demand per area per certain time period (e.g. 1 year). In case of cold-spots, PV supply is insufficient to meet the building's electrical load demand. Power is then taken from the grid in case of grid-connected PV system. In the contrary case, feed-in tariffs allow to sell electrical power surplus to the national grid, if the electric power of the installation is above a certain value (Mondol, Yohanis, & Norton, 2006). Energy self-sufficiency takes place when the energy demand is covered by the energy generated.

1.3 Research objective and research questions

The aim of this research is to assess the potential benefits of urban scale PV systems with use of GIS and LIDAR data expressed in rooftop solar radiation map, hot-spots/cold-spots and percentage self-sufficiency per postcode areas.
The research starts with literature review of previous solar potential studies and parameters and data selection.
The outcome of this thesis can support on-site renewable energy generation in Wageningen. It can be beneficial by guiding private investors as well as local authorities to determine which parts of the existing built-up area can be used for solar energy generation in order to be cost effective, and in which parts use of solar panels would not be economically profitable.

Research objective

Estimate electrical self-sufficiency in case of roof-top photovoltaic in the city of Wageningen by the analysis of LIDAR data.

Research questions

RQ 1 – Which local conditions, building characteristics and weather conditions influence the electricity generation potential?

- Which parameters and data sources are used in current solar potential studies?
- Which data are available for calculation of solar potential in Wageningen?
- What roof characteristics have to be taken into consideration and how can these characteristics be derived from LIDAR (AHN2) data?

RQ 2 - What is the annual potential local energy supply by PV solar collectors calculated based on selected local conditions, roof characteristics and weather conditions?

- What is the electricity potential within 4-digit postcode areas?
- What is the electricity potential within 5-digit postcode areas?
- What is the electricity potential within a city of Wageningen?

RQ 3 – What is the impact of tree shading on solar potential?

- What is the impact of tree shading on solar potential in the city center?
- What is the impact of tree shading on solar potential in a residential area?

RQ 4 – In how far can 5-digit postcode areas in Wageningen become self-sufficient in terms of electricity supply?

- What are the hotspots (sites with prevailing supply) and cold-spots (sites with prevailing demand) in selected 4-digit and 5-digit postal code areas?

1.4 Thesis structure

This thesis consists of six chapters. Chapter one gives background information, problem definitions and research objective.

The second chapter includes the literature review, overview of parameters and data used in current solar potential studies and provides a selection of important parameters influencing PV potential to be used in answering question 1.

Third chapter describes materials and methods.

Chapter four illustrates the results as obtained in case of answering questions 1, 2, 3 and 4.

Chapter five represents the validation of method and results.

The discussion chapter corresponding to results is given in chapter six.

Conclusions and recommendations are presented in chapter seven.

2 Literature review

Literature study is an essential part of this master thesis. Based on a survey on data and methods of existing studies, maximum number of relevant parameters used in surveyed studies is identified.

The amount of generated electricity is determined by availability and amount of solar radiation and parameters affecting PV cell efficiency (Bourget, 2013). These parameters are the sites latitude, orientation, weather conditions, roof tilt, air temperature, shadow effects and module efficiency. The conversion efficiency mainly depends on the solar irradiation and operating temperature.

2.1 Current state of determining PV potential via GIS/LIDAR

Spatial/Temporal resolution of meteorological data

Voegtle (2005), Kassner (2008) and Jochem (2009) did not use any meteorological data since their studies focused only on roof selection. However for roof-top PV potential analysis meteorological data are necessary in order to calculate solar irradiance. The spatial and temporal resolutions of meteorological data of selected studies differ: Brito (2011) and Hofierka (2009) used solar radiation information from PVGIS (thorough description in chapter 2.3.2). Most of the meteorological data have a monthly temporal resolution. Wittmann (1997) used climatic spatial data and monthly average daily radiation data. Izquierdo (2008) used monthly irradiation maps with a spatial resolution 200x200m, also Santos (2011) applied the analysis on a monthly basis. Wiginton (2010) did not use any spatial radiation data for its unavailability.

Shortcomings of studies

Jochem mentions problems with processing of large area LIDAR point clouds since the data processing is limited by computer´s memory (Jochem, Höfle, Wichmann, Rutzinger, & Zipf, 2012). According to Voegtle et al. (2005), Kassner (2008) and Santos et al. (2011) point density in LIDAR data can be insufficient since partially roof patches cannot be detected and not all disturbing elements (e.g. overhangs, dormers, chimneys, antennas etc.) were excluded. Jochem et al. (2009) noted difficulties with distinguishing points on buildings and vegetation points which led to overestimation of suitable area. Kassner identified an approx. 1.5 m wide band along roof borders and also roof with displaced points (and pointed out the necessity of caring of misplaced points which affect the modeling of outlines). Voegtle recommends

use of supplementary aerial images which would support more precise detection and delineation of roof areas (Voegtle, Steinle, & Tovari, 2005).

Hofierka & Kanuk note that the calculated potential includes large spatial and temporal variations caused by global (global irradiance) and local factors (sky-view obstructions, temperatures) (Hofierka & Kaňuk, 2009). These temporal and seasonal nature of solar irradiation and electricity demand must be considered (Wiginton, Nguyen, & Pearce, 2010). When power demands do not match PV power generation, energy storage capacities are necessary. Times of highest power demand (winter) does not correspond to the times of highest solar flux.

Electricity demand cover

Electricity demand cover differs mainly based on geographical location. Brito et al. (2012) estimated a total PV potential of the 538 identified buildings in Lisbon suburbs to be around 11.5 GWh/year which covers approximately 48% of the local yearly electricity demand. Jochem et al. (2009) performed solar potential analysis for urban settlement in the city of Feldkirch with an area of approximately 1 km x 1 km. His method detected a subset of 809 out of 1,071 roof planes where the arithmetic mean of the annual incoming solar radiation exceeded 700 kWh/m^2. Kassner (2008) predicted a solar harvest of 100 kWh/m² per year for photovoltaic modules on 13 buildings within the urban campus of the University of Cologne, Germany. Hofierka & Kaňuk (2009) estimated that rooftop photovoltaic potential could cover about 2/3 of current electricity consumption in the Bardejov, mid-sized city in Slovakia. Jo & Otanicar (2011) estimated the PV potential of commercial and government buildings in a 10.36 km^2 area located in the city Chandler, Arizona. This study showed that calculated electricity production of 18 600 MWh would cover about 10% of the total electricity demand of all the buildings in the case study area. Ruiter (2011) determined solar energy potential estimation based on a 3D city model of a small area in Groningen. His study showed that 10% of the roof surfaces used for solar panels would meet more than 50% of the energy demand. The overview of data acquisition methods, data characteristics and outcome of the studies is stated in section Physical parameters.

2.2 Physical parameters

Physical parameters affecting solar potential used in surveyed studies are: latitude, aspect, weather conditions, roof tilt, air temperature, shadow effects, module efficiency. Their use in recent solar potential analysis studies is given in Table 1.

Table 1: Selected parameters for roof solar potential analyses from different authors

Author/parameters	Atm. effects	Latitude	Tilt	Aspect	Sun angle shifts	Shading of buildings and terrain	Rad. components	Excl. segments	Temperature	Veg. shading
Wittmann et al. (1997)			√	√			√			
Voegtle et al. (2005)			√	√						
Kassner. et al. (2008)			√	√		√				
Izquierdo et al. (2008)	√	√	√	√		√	√			
Jochem et al. (2009)	√		√	√		√	√			√
Hofierka and Kaňuk (2009)			√	√	√	√	√			
Wiginton et al. (2010)				√		√		√		
Brito (2011)	√	√	√	√	√	√				
Santos (2011)	√	√	√	√	√	√				
Nguyen and Pearce (2012)	√	√	√	√	√	√	√			
Kodysh et al. (2013)	√	√	√	√	√	√				
Lukač et al. (2013)	√	√	√	√	√	√	√	√		√
Hsieh et al. (2013)	√	√		√	√	√	√			
Jakubiec and Reinhart (2013)	√	√	√	√	√	√	√		√	√

Sun and Solar Radiation

With a growing solar irradiance the electricity yield increases. Solar radiation is received throughout the year and changes its composition due to scattering, diffusion and absorption in the atmosphere.

Solar constant S_{Const} stands for the solar radiation reaching the top of the Earth's atmosphere at the mean earth-sun distance (Figure 4). S_{Const} is also called the solar constant, but this term is rather misleading, since the solar irradiance at the top of atmosphere varies with the sun activity (luminosity) and distance of the Earth relative to the Sun (Bourget, 2013).

According to the World Radiation Center (WRC) the solar constant is 1367 W/m^2 ("WRC," 2013).

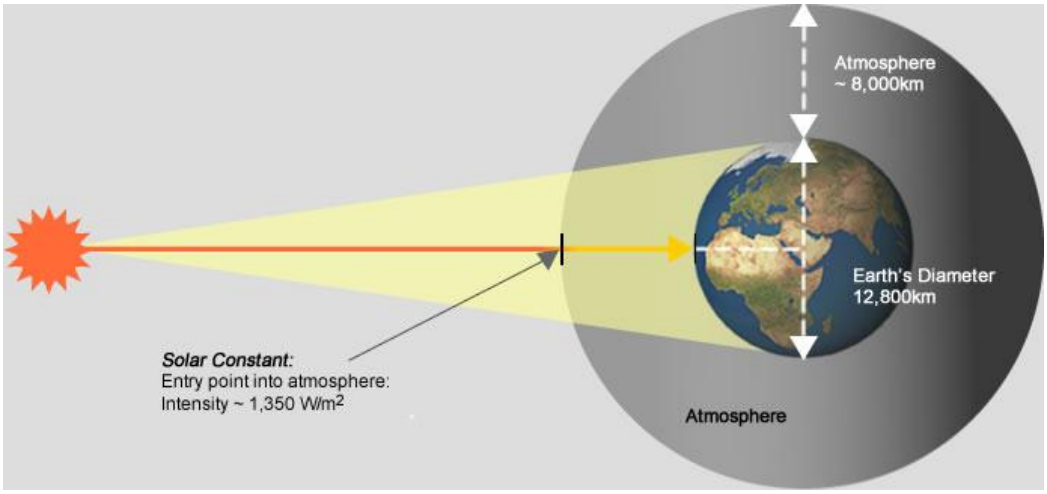

Figure 4: The intensity of solar irradiation directly outside the earth's atmosphere on a horizontal surface so called "solar constant" ("Green Rhino Energy," 2013)

The extra-terrestrial radiation rate varies seasonally due to the variation in distance between the earth and the sun over a year. This value must be corrected for a respective day of the year and latitude.

Radiation components

As seen on Figure 5, three components of solar radiation can be distinguished at the surface: direct beam, diffuse and reflected solar radiation. Direct beam radiation reaches the solar collector directly without being reflected by the atmosphere. Diffuse radiation hits the receiver after being scattered by molecules and particles in the atmosphere. Reflected radiation is sunlight that has been reflected off of non-atmospheric things such as the roof in front of the collector. All three components contribute to solar energy collection but reflected radiation does not belong to significant part of the sunlight striking solar panels (Masters, 2004).

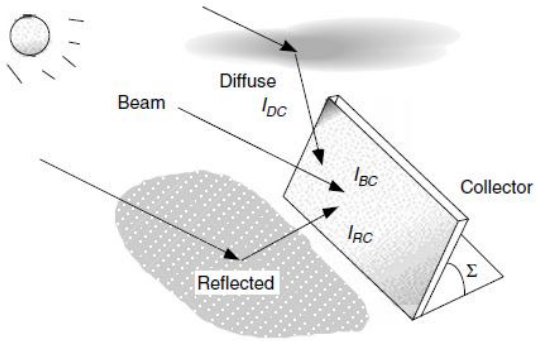

Figure 5: Solar radiation striking a collector consisting of three components: direct beam (I_{BC}), diffuses (I_{DC}), and reflected (I_{RC}) radiation (Masters 2004).

Atmospheric effects
Irradiation is also modified by atmospheric conditions (e.g., clouds, aerosols, water vapor, and ozone) (Hofierka & Kaňuk, 2009). Sky conditions can be characterized by the clearness index and ratio of diffuse radiation to total global solar radiation. Optimum output can be achieved only with full sun and no clouds. Based on the type and percentage of cloud cover the output can vary significantly. Under cloud cover, solar irradiance can be reduced up to 60% of the peak of solar irradiance in seconds (GEN, 2013). Three-fifths of the sky is clouded on an average day in the Netherlands (Heslinga, Meijer, Rowen, & Wintle, n.d.).

In some analyses (Kodysh, Omitaomu, Bhaduri, & Neish, 2013) the clearness index and the ratio of diffuse radiation are fixed, constant values throughout the year, which can impact the calculated annual solar radiation. In case of Solar Analyst toolbox it is advisable to divide the analyses, at least, into the monthly step.

Sun angle shifts
Solar radiation components contribute differently according to different latitudes and times of the year in a predictable cycle. In higher latitude sites diffuse radiation ratio is generally higher during winter than in summer. On the contrary, sites with lower latitude have less seasonal variation. For instance in sunniest month in London, UK (51° North) about approximately 50% of total radiation is diffuse. In winter diffuse radiation represents by far the majority of total radiation. Oppositely in Aden, Yemen (19.5° North) 30% of the radiation is diffuse in the sunniest month and in December this number increases only to 35% (Palz, 1983). Further, small variation of the solar irradiance is caused by the changing Earth-Sun distance, which varies sinusoidally since the orbit of the Earth around the Sun is an ellipse (Bourget, 2013).

Shadow and elevation
Shading of roof structures and surrounding objects is very common in urban areas. Shadowing effects blocks direct radiation, which can reduce the output energy by 25% (Gross, 1997; Norton et al., 2011). Accordingly solar panels should be situated on places, where they will never be shadowed. There is no threshold for acceptable length of shadow duration. With quickly growing PV technologies the tolerance to shadow has increased (Norton et al., 2011).

Latitude
The optimum array angle installation depends on the latitude of the site. In lower latitudes (close to equator) maximum output is obtained when the module angle is approximately equal to latitude whereas in higher latitudes (such as in northern Europe) the difference between the latitude angle and the optimum tilt angle rises (Siraki & Pillay, 2012).

Aspect
If possible, roofs should be oriented directly towards the equator, facing south in the northern hemisphere. A true south orientation is the most effective, but the solar PV array should

be orientated between south-east and south-west. In these cases only small percentage power loss (up to 5%) occur (Masters, 2004).

Efficiency

The efficiency of energy conversion is mainly influenced by the PV panels itself (Singh, 2013). Besides that the performance of PV module is affected by a variety of factors influenced by exposure of PV cells to dust and temperature and humidity (Charabi & Gastli, 2013; Mekhilef, Saidur, & Kamalisarvestani, 2012).

Temperature of solar cell

Temperature can affects electrical efficiency of a PV cell/module considerably. With increasing temperatures the efficiency of photovoltaic solar cells decrease (Kumar & Rosen, 2011; Tyagi, Rahim, Rahim, & Selvaraj, 2013). Solar radiation together with high ambient air temperature can make the effect of heating up the roofs even stronger than ambient air temperature itself (Jakubiec & Reinhart, 2013). The relationship between temperature and efficiency varies with cell material. The factor of temperature is important since the conversion efficiency decreases when the temperature of the PV cell is above 25 ˚C (Nishioka et al., 2003). Factor of temperature is not taken into analysis because of unavailable data however it is included in discussion.

Conversion efficiency

Every PV-module has to be connected to an inverter. The inverter is critical component in a photovoltaic system, converting (voltage) and processing the electricity. It converts the direct current (DC) power produced by solar PV panels to alternating current (AC) that can be used in homes or fed into a commercial electrical grid (Notton, Lazarov, & Stoyanov, 2010). Electronic technique called Maximum Power Point Tracking (MPPT) allows catching the maximum power through adjusting the voltage and current supplied from the PV panel.

Inverter efficiency measures power out of the inverter as a percentage of the power into the inverter. Inverter efficiencies differ however in general Solar PV inverters are highly efficient, state-of-the-art inverters reach peak efficiencies in the 95–97%. Optimal sizing and inverter type must be chosen according to application (Burger & Ruther, 2005).

Effect of humidity on solar cells

Humidity refracts, reflects and diffracts the direct visible solar radiation (Gwandu & Creasey, 1995), besides that it lowers solar cell efficiency through hydrolysis of polymeric components, corrosion of glass and of metallic components (e.g. grids and interconnectors) (Koehl, Heck, & Wiesmeier, 2012; Mekhilef et al., 2012). The property usually measured is the relative humidity. According to Britannica encyclopedia, relative humidity is “a ratio of the actual vapor pressure of water in the air to that in air saturated with water vapor. This value it is often expressed as a percentage” (Encyclopaedia Britannica, 2013). Average annual relative humidity in the Netherlands is 77.3% (“Climatemps,” 2013).

Effect of dust on solar cells

Dirt and dust accumulating on the PV module surface can considerably reduce the electric energy output (up to 43%) and cells efficiency due to blocking of the coming irradiance onto PV modules (El-Shobokshy & Hussein, 1993; S. a. Kalogirou, Agathokleous, & Panayiotou, 2013; Mani & Pillai, 2010; Sarver, Al-Qaraghuli, & Kazmerski, 2013). According to Jiang et al. (2011), solar cells´ efficiency decreases linearly with growing dust deposition density. In other words PV surface need to be clean to maintain the performance.

There are active sand dunes in the Hoge Veluwe area near Wageningen. These dunes might bring some sand particles to Wageningen. Also the very fine sand from the Sahara can be blown all the way to Europe. The effect of these particles is not taken into account, since it is assumed that frequent rain (217 rainy days per year) cleans the collector surface sufficiently (Mani & Pillai, 2010).

Tilt

According to Duffie & Beckman (1991) the optimum tilt angle of the collector equals to the latitude of the location with angle variations of 10–15˚. Since the optimum tilt angle varies during different months of the year (Tanaka, 2011), it is recommended to use slightly higher angle for improving efficiency in winter and slightly smaller angle for improving efficiency in summer (S. Kalogirou, 2003; Masters, 2004).

Building-integrated solar energy collection is accomplished by integrating solar energy collectors either into building facades or roofs. Their positions strongly affect performance of the solar PV array. Output of horizontal PV modules as well as south-facing vertical modules decreases (Hussein, Ahmad, & El-Ghetany, 2004).

Data Sources

Due to increasing quality and availability, and decreasing costs of LIDAR-data it is possible to extract rooftops of individual houses by DTM and DSM derived from the LIDAR data. Based on this detailed level up scaling information to a range of applications to analyze solar potential.

Since the study works with fine resolution (0,5 m) and large area (32 km^2) overview of data acquisition method, data characteristics and outcome of the studies was made for comparison (Table 2). Large number of studies estimated the roof area available for photovoltaics and estimated its solar potential, others address the selection of the roof planes and its segments that are favorable for photovoltaics. Spatial resolution is stated only in cases raster data are used, LIDAR point density is stated when known.

Table 2: Characteristics and acquisition methods of input spatial data and way of presenting outputs

Author/parameters	Spatial data acquisition	Spatial data characteristics	Visualization, Output
Wittmann et al. (1997)	Roof areas: photogrammetry	Extent: 1.08 km^2	Non-spatial, monthly solar radiation energy (GWh)
Voegtle et al. (2005)	DTM: LIDAR Roof areas: cadaster	Extent : 8 km^2 resolution: not stated	Roof selection
Kassner. et al. (2008)	DTM:LIDAR the average point density 1 point/3-4m2 (after filtering) Roof areas: photogrammetry	Extent: 13 buildings within the urban campus of the University of Cologne, Germany	Roof selection
Izquierdo et al. (2008)	DTM: SRTM3 Roof areas: cadaster	Extent: Spain (~500 000 km^2) Resolution: 200m x 200m	Spatial, regions rooftop solar potential (GWh/year)
Jochem et al. (2009)	DTM: LIDAR (17 points/m2) Roof areas: LIDAR	Extent: 49 km^2 Resolution: 1m x 1m	Roof selection
Hofierka and Kaňuk (2009)	DTM: topographic maps (contours) 1:10 000 Roof areas: otrophotomap vectorization + laser distance device	Extent: 3,7 km^2 Resolution: 1m x 1m	Spatial, rooftop solar radiation maps (kWh/m2). Annual solar radiation energy (GWh).
Wiginton et al. (2010)	Roof areas: automated/manual digitalization of otrophotomap (vectorization)	Extent: 48 000 km^2	Non-spatial, annual solar radiation energy (GWh)
Brito (2011)	DTM: LIDAR (1 point/m2) Roof areas: building footprints (source not stated)	Extent: 0,085 km^2	Spatial, annual rooftop solar radiation map (kWh/m2). Annual solar radiation energy (GWh).
Santos (2011)	DTM: LIDAR Roof areas: building footprints vector layer 1:1000	Extent: 6,25 km^2 DTM derived from LIDAR Resolution: 1m x 1m	Spatial, map of energy produced annually at the roof-tops (MWh).
Nguyen et al. (2012)	DTM: LIDAR (1,91 point/m2) Roof areas: LIDAR based + roof print vector layer	Resolution: 0.55m Extent: 1 km^2	Spatial, annual rooftop solar radiation maps (kWh/m^2)
Kodysh et al. (2013)	DTM: LIDAR Roof areas: building footprints vector layer	Extent: 847 km^2 (212,000 buildings) Resolution: 1m	Spatial, monthly rooftop solar radiation maps (kWh/m^2)
Lukač et al. (2013)	DTM: LIDAR Roof areas: LIDAR based	Extent: 1 km^2 Resolution: 1m x 1 m	Spatial, annual rooftop solar radiation maps (kWh/m2)
Hsieh et al. (2013)	building model	Extent: 288000 m^2, no resolution	Non-spatial, annual electricity demand coverage (%)
Jakubiec and Reinhart (2013)	3D model: LIDAR (6,84 point/m^2)	Extent: 18,5km^2	Spatial, annual rooftop solar radiation maps (kWh/m^2)

2.3 Summary of findings

Based on the literature review, four groups of parameters defining the interaction of the solar radiation with the earth's atmosphere and surface were found.

All these parameters are considered in the later analysis.

1. *Local conditions*
- geographic location (position of the area relative to the sun angle shifts), shadow

2. *Building characteristics*
- tilt, roof surface, aspect, building height

3. *Weather conditions*
- Solar radiation and radiation components, atmospheric effects

4. *Technical parameters*
- Cell efficiency

Relative humidity, temperature, dirt and dust particles were not included in the analysis. A number of parameters (e.g. tilt, slope, height, orientation) can be derived from LIDAR data. From previous research it is obvious that accuracy of available data affects the quality of derived parameters. With increasing accuracy of LIDAR data together with new methods for roof segmentation (Jochem, Höfle, Rutzinger, & Pfeifer, 2009; Kassner, 2008; Voegtle et al., 2005) it is possible to derive these parameters more precisely.

Rooftop solar radiation map represents a suitable outcome of solar analysis since they offer a way of present both geographic distribution and intensity on a rooftop (Kodysh et al., 2013). Intention of this study is to create rooftop solar radiation map depicting individual building solar radiation potential based on mentioned parameters.

The rooftop solar radiation maps raise a research opportunity. For example house owners tend to plant trees nearby their houses for its cooling effect in summer months (Akbari, Kurn, Bretz, & Hanford, 1997; Sawka, Millward, Mckay, & Sarkovich, 2013). As visible in Table 3 only three of the introduced studies considered influence of tree shading (Jochem, Höfle, Hollaus, & Rutzinger, 2009; Lukač et al., 2012). The influence of shade on the solar access of buildings has been already studied in California (Levinson, Akbari, Pomerantz, & Gupta, 2009) and in a district of North Vancouver (Tooke, Coops, Voogt, & Meitner, 2011). The computed reduction of total solar radiation received by residential building rooftops of these studies differs significantly. One of the aims of this study is to find out whether the tree shading in Wageningen is relevant or this aspect can be neglected.

3 Materials and Methods

3.1 Conceptual framework of methodology

The framework of this thesis is shown in Figure 6. Selection of parameters influencing the PV electricity generation potential was first carried out and rooftops were selected from LIDAR data (RQ1). Based on local conditions, roof characteristics and weather conditions yearly technical potential of roof-top photovoltaic energy production of solar energy was computed (RQ2). With use of AHN2 data trees shading impact on roof electricity potential was evaluated (RQ3). Based on computed annual electricity potential and annual electricity demand hot-spots and cold-spots within 4-digit and 5-digit postcode areas and percentage self-sufficiency within 5-digit postcode areas were determined (RQ4).

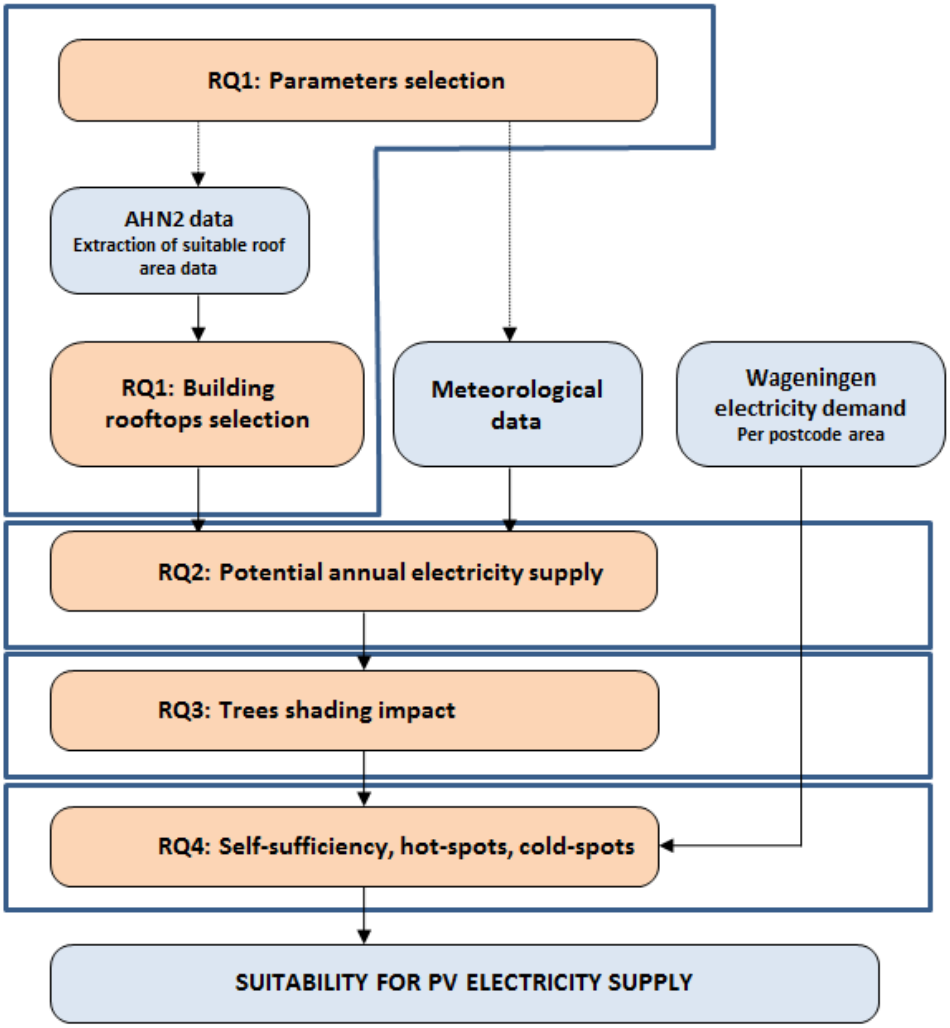

Figure 6: Data collection and processing framework. Full arrows represent data flows. Dotted arrows represent information flows. Blue boxes are external data and red boxes are calculated or processed data.

3.1.1 Study area

The area of interest is located in municipality of Wageningen (51° 57′ 52″ N, 5° 39′ 47″ E) (see Figure 7) and covers an area of 32 km^2. Three different scales were used - level of whole municipality and on level of 4-digit (9) postcode areas and 5-digit (64) postcode areas. Wageningen's built surface area is 6.73 km^2 (googleearth.com, 2012). Total area of roofs in Wageningen covers 1.67 km^2. Besides single houses Wageningen is comprised of block buildings, university with research institutes and many office buildings with large flat roof areas.

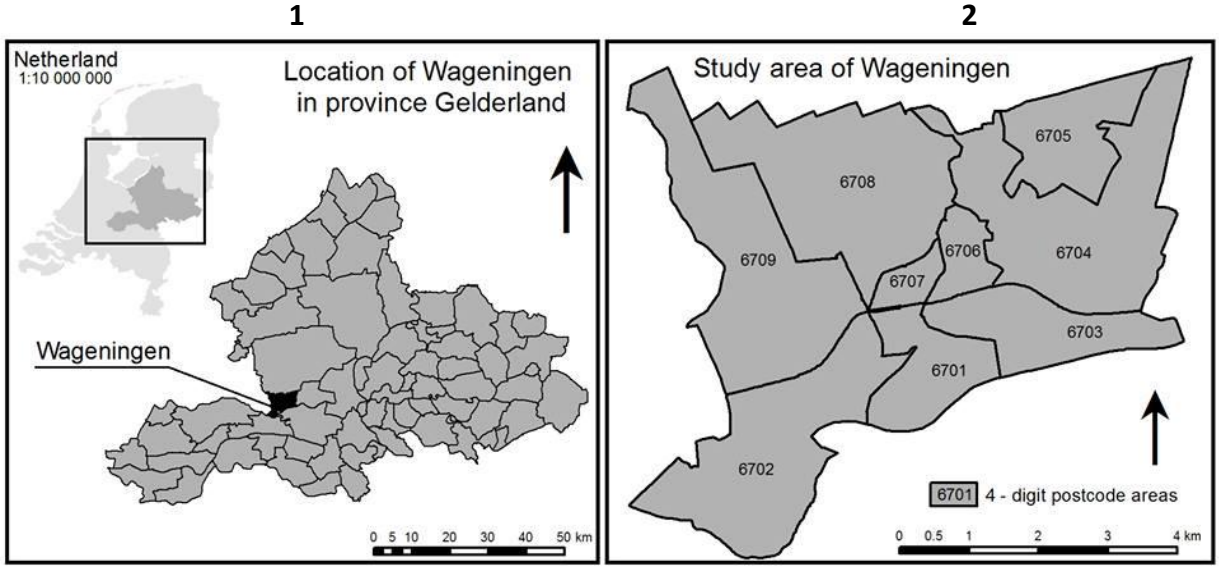

Figure 7: Location of study area. Wageningen. Location of Wageningen in province Gelderland (1) Wageningen divided into 4-coded postcode areas (2)

The Netherlands has a moderate maritime climate influenced by the North Sea and the warm Gulf Stream (Heslinga et al., n.d.). Relative humidity in the Netherlands is on average year is as high as 77.3%. This factor is being neglected in current research therefore it was not considered in the analysis. The average temperature in the Netherlands is 2 °C in January and 17°C in July (Heslinga et al., n.d.). High share of diffuse radiation causes low insolation (Šúri et al., 2007).

3.1.2 Data description

For this thesis four different data sources are used: firstly, LIDAR data AHN2, secondly meteorological data from PVGIS database and a weather station in Wageningen (WUR), thirdly electricity demand data from Energy Atlas Wageningen (Liander, 2010) and lastly postcode areas, The Key Register for Addresses and Buildings ('BAG') and monuments. All other data used in this research is derived from these sources.

Climatic data

PVGIS

Project PVGIS (Photovoltaic Geographical Information System) was developed in Joint Research Centre of the European Commission. It is a research GIS oriented tool for the performance assessment of solar PV systems in European geographical regions (see Figure 8). PVGIS as a solar radiation database offers geographical grid resolution 1 km × 1 km. It was developed from climatologic data homogenized for Europe and available in the European Solar Radiation Atlas and combines measured and modelled elements. PVGIS is based on r.sun model. It is freely accessible on the web at http://re.jrc.ec.europa.eu/pvgis/.

Figure 8: Long-term average global radiation (Šuri et al., 2007)

According to Hofierka & Šuri (2002) PVGIS dataset had confirmed to be very effective in describing European solar irradiation (JRC, 2012). PVGIS provides directly averaged monthly proportion of global normal radiation flux that is diffuse for each month in year (JRC, 2012).

Weather station Haarweg

The weather station of Meteorology at the Haarweg, Wageningen provides data available in high temporal resolution for free. These data contains the temperature [°C] and radiation in [W/m^2] for long wave, shortwave and diffuse radiation. The resolution of this information is both on hourly and daily basis, and the data used are from the years 2008 until 2012 (WUR, 2003).

LIDAR data

- AHN2 (2010) (detailed and precise LIDAR database).

  - 19,5 points per m^2
  - Precision: 5 cm

The AHN (actual height model of the Netherlands) is a very detailed and precise LIDAR database (Zon, 2011). The AHN data was initially acquired for water and flood management, however it is used in multiple applications like police areas, solar cadasters, archaeology and 3D games (Rijkswaterstaat Bestuursstaf, 2013). The first version of this data (AHN1) was measured between 1996 and 2003. As shown in
Figure 9 between 2007 and 2012 due to newer techniques more detailed and precise height model of the Netherlands (AHN-2) was made (6-10 points/m^2) (Zon, 2012).

Figure 9: AHN2 scanning of the whole Netherlands . source: Zon, 2010. Red point marks Wageningen

Detailed topographic data such as rooftop, roof slope and roof orientation can be obtained from Digital Surface Models (DSM) which can be derived from airborne LIDAR scans. Digital surface models are dependent on measurement density, accuracy of the laser scanner system and post-processing software. With use of GIS, features such as tilt, orientation, surface and elevation can be derived based on DSM. According to Kodysh (2013) to derive mentioned characteristics, horizontal spacing in LIDAR point cloud should not be greater than 1 m. Roof elements such as roof overhangs, chimneys, dormers, and antennas should not be overlooked. However, in order to detect roof artifacts like roof overhangs, chimneys, dormers, antennas, higher point cloud density or additional spectral information are needed (Santos, Gomes, Brito, & Freire, 2011). Delineation of the roof plane boundaries derived from LIDAR data is not very precise, therefore regularization techniques application are necessary (Rottensteiner, Trinder, Clode, & Kubik, 2005).

Energy demand data

The energy demand coverage of Wageningen is evaluated based on the E-atlas ("energy atlas") as seen in Table 3 (Liander, 2010). This energy atlas was provided by Liander for the Municipality of Wageningen and is based on actual demand data. It contains electricity consumption of households, catering and companies per district or postcode area for year 2008. For this study the electricity total consumption of households and companies is used.

Table 3: Total energy consumption per postcode in Wageningen. Source: E-atlas 2008

postcodes Wageningen	Total electricity consumption (MWh)
6701	17 281
6702	26 699
6703	20 026
6704	2 554
6705	3 214
6706	10 515
6707	8 677
6708	51 834
6709	18 483

Postal code areas

BridGis data provide administrative selections on 4 -, 5 - and 6-digit level. Electricity yield is computed based on 4- and 5-digit postcode areas. Due to data availability limitations, 4-digit postcode areas from year 2008 and 5-digit postcode areas from year 2006 were used in this study.

Division of the districts in the CBS database and in the E-atlas do not match for all districts (CBS includes 14 districts for the City of Wageningen while in the E-atlas Wageningen is split up in 20 districts). Therefore 4-digit and 5-digit postcodes representing the smallest possible scale were used.

Cadastral data

The buildings (houses) data layer was given by Basisregistraties Adressen and Gebouwen (BAG) from Dutch Cadaster. Changes of cadaster information are being updated by aerial photographs (Kadaster, n.d.). Since cadastral data from 2008 and 2012 were found identical, the data from 2012 were used.

Monumentenregister

The National Monuments datasets contain data of all monuments in the Netherlands designated as a protected monument. This data can be viewed via online Memorial Register (Rijksdienst voor het Cultureel Erfgoed, n.d.). The study are contains 59 national monuments, examples can be seen in Figure 10.

Figure 10: Examples of national monuments in Wageningen. Laboratory of Horticulture, Grote Kerk, De Bovenste Polder (former brick factory). source: Wikipedia, n.d.

3.1.3 Input calculation parameters

Characteristics of atmosphere

- Transmissivity of atmosphere or "clearness index"
- Diffuse proportion

Data description

Considerable attention is given to the calculation of input atmospheric parameters. The atmospheric parameters are input data, which values significantly affect the result. Atmospheric processes are taken into account with use of *diffuse proportion* factor and t*ransmissivity of atmosphere*.

Diffuse proportion D/G is calculated as a proportion of global normal radiation flux (incoming shortwave radiation) that is diffuse (ESRI, n.d.-a; Fu & Rich, 1999). For determination of the diffuse proportion, PVGIS and Haarweg meteostation data were compared. There were only slight variations of diffuse proportion between both sources, so only Haarweg data were used in the analysis.

Transmissivity or clearness index is a property of the atmosphere. It is defined as a ratio between the surface measured direct beam irradiance *(*$S\downarrow$*)* and the extra-terrestrial solar radiation on a horizontal surface extra-terrestrial solar irradiance (***H***$_0$) (Zangvil & Aviv, 1985).

The equation given is $\tau = S\downarrow / H_0$ (Baigorria, Villegas, Trebejo, Carlos, & Quiroz, 2004)

where τ = transmissivity, S↓ (W/m²) is the measured incoming shortwave radiation, H_0 (W/m^2) is solar constant corrected for respective latitude.

The extra-terrestrial solar radiation $\boldsymbol{H_0}$ on a horizontal surface can be calculated from the following equation:

$H_o = (I_o/\pi)[\omega_s(\sin\phi)(\sin\delta) + (\cos\delta)(\cos\phi)(\sin\omega_s)]$

where: I_o - extra-terrestrial irradiance in kW/m^2, I_{sc} – Solar constant (I_{SC} = 1367 W/m^2), N - day number in the year (N=1 on January 1st and N=365 on December 31st), ϕ – local latitude (ϕ = 51,969187), δ – solar declination angle, ω_s = Sunrise hour angle, E_o - eccentricity correction factor of the earth´s orbit.

The extra-terrestrial irradiance in kW/m^2 can be calculated from the following equation

$$I_0 = I_{SC}\left[1 + 0.033\cos\left(\frac{N}{365}\times 360°\right)\right]$$

ω_s = cos-1[-(tanϕ)(tan δ)]

$$\delta = 23.45°\sin\left[\frac{N+284}{365}\times 360°\right]$$

E_o = 1+0.033cos (360N/365)

Both average monthly values of diffuse ratio and average monthly values of clearness index were calculated from daily data of years 2008-2011 measured at the Haarweg weather station. Year 2012 is not included because of incomplete data. Both calculated parameters – diffuse ratio and clearness index - are provided in Appendix 2.

3.2 Data processing

3.2.1 RQ 1: Literature review selection, building footprints

Selection based on literature review

The intended outcome was an overview of parameters affecting the roof solar potential. Most of the reviewed articles are selected form the leading journals in the field of solar energy research (*Solar energy, Renewable energy and Computers, Environment and urban systems*), other relevant articles from other journals were included as well.

LIDAR data processing, building footprints

LIDAR data is extremely large. The received LIDAR data of whole Wageningen and surroundings occupied 21.5GB of disk space. Raw LIDAR data was clipped for Wageningen and for its easier manipulation the whole area was divided into 4-coded postal code areas. Used size of the areas met the limits for free use of LAS Tools and this division was used for following steps of the analysis (if allowed by computer memory limitations).

The AHN2 airborne LIDAR data (21,5 B) had been pre-processed already, having information of return numbers, return time, coordinates, etc. Since the research targets points representing the trees and the buildings were filter out. The classification was done by tools from LAStools (see Figure 11).

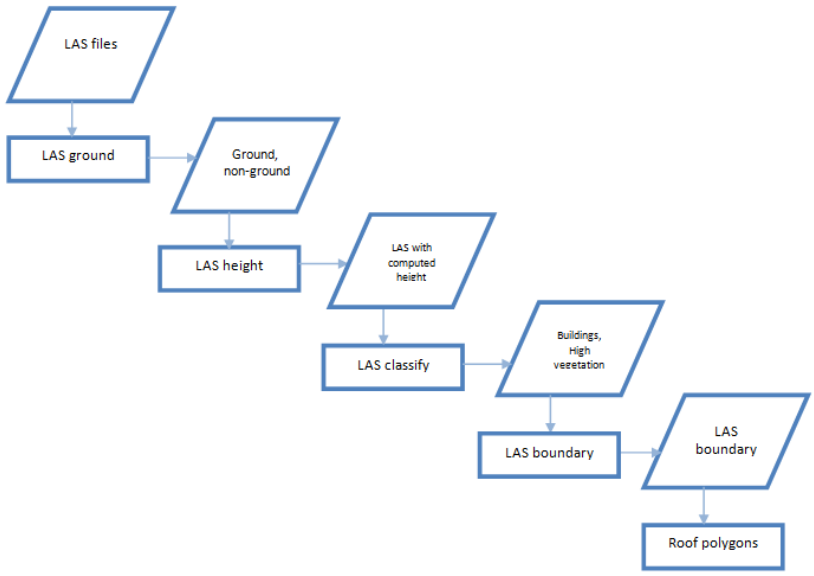

Figure 11: Classification process by using LAStools

By using the „LAS ground“ tool the original LIDAR points were classified into ground points (class = 2) and non-ground points (class = 1). Depending on the topography and the building characteristic, two pre-defined settings have been used: “towns or flats“ setting were used for most of the Wageningen, but for same industrial parts of the city (42 tiles), setting was changed to “cities and warehouses”.

The height of each point above the ground was computed by „LAS height“ tool and in order to compress the file points below -2 and above 70 meters were dropped.

The ground classified points identified in previous step are used to construct a ground TIN. Elevation of ground is zero while other points have an elevation that equals their height above the ground TIN.

The “LAS classify” tool classifies buildings and high vegetation (trees). The tool essentially tries to find neighboring points that are at least 3 meter above the ground (ground offset=3). This is done in order to avoid incorrectly positioned points and therefore overestimation of the insolation on the edges of the roofs. Subsequently the tool is set in order to form planar=0.1 (roofs) or rugged=0.4' (trees) regions. The building roofs were detected in a way that gutters were included. Tiny buildings which are not suitable for PV installation were excluded.

Since automated classifications carried out on LIDAR data does not classify all the points correctly (i.e. wrongly classified points representing trees) (ESRI, 2012) (Figure 12), manual classification and data cleanup was performed using standardized classification codes (Figure 13).

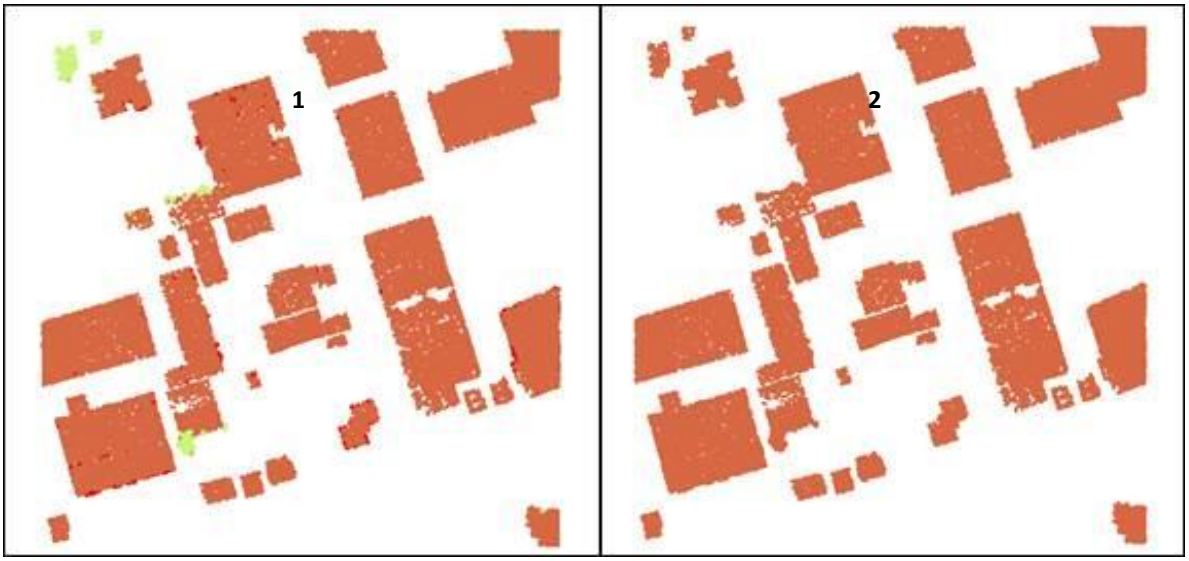

Figure 12 : Point cloud before (1) and after (2) reclassification. Green color represents trees and red represent a noise

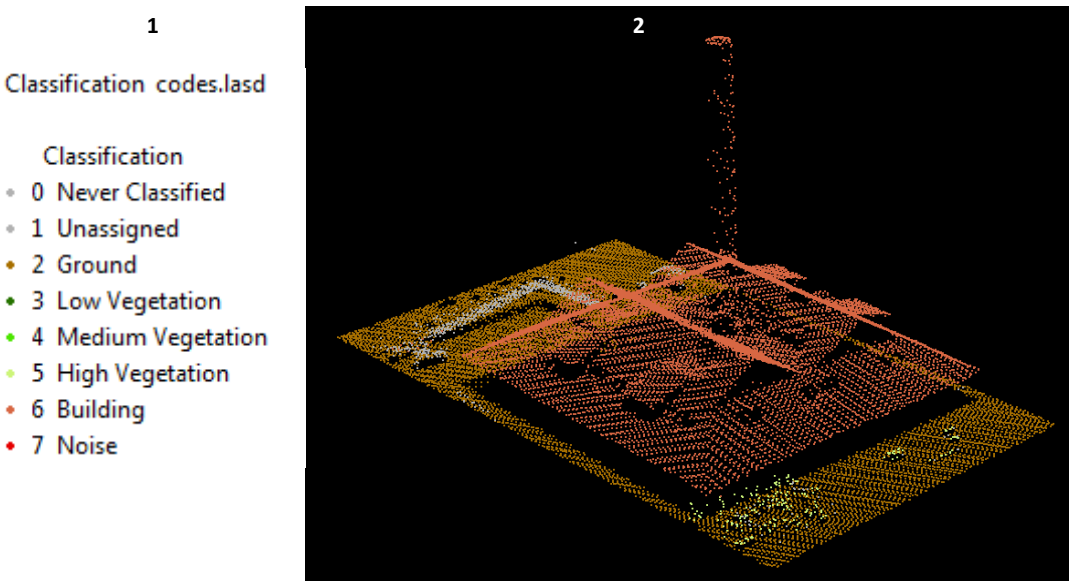

Figure 13: Classification codes for LAS files defined by the American Society for Photogrammetry and Remote Sensing (ASPRS) (1). Correctly classified brick factory (2).

The classified LIDAR data were divided into two parts through "las2las" function - one part represented buildings and second part represented all other points. In the first part, points which were miss-classified as buildings (=6) were corrected (reclassified into noise (=7) or trees (=5) if necessary). Noise was filtered out (drop 6) and the two parts were merged again together in LAS tools.

Finally, with correctly classified point cloud the "LAS boundary" tool (concavity=1,5) were used to compute building foot prints - boundary polygons that encloses the points. In order to simplify the shapes optimally and remove buildings smaller then set threshold of building footprints *Simplify building* and subsequently *Simplify polygon* function with simplification tolerance of 1 m and minimum area 10 m^2 were used. Since most of the buildings have straight lines, POINT_REMOVE algorithm keeping the essential shape of a line while removing all other points was used for building simplification was set.
This setting lead to simplification of buildings, buildings smaller that set minimum area after the simplification process were removed from the output feature class.

Figure 14 compares changes of building footprints before and after simplification. Eventually simplified buildings were manually edited when necessary.

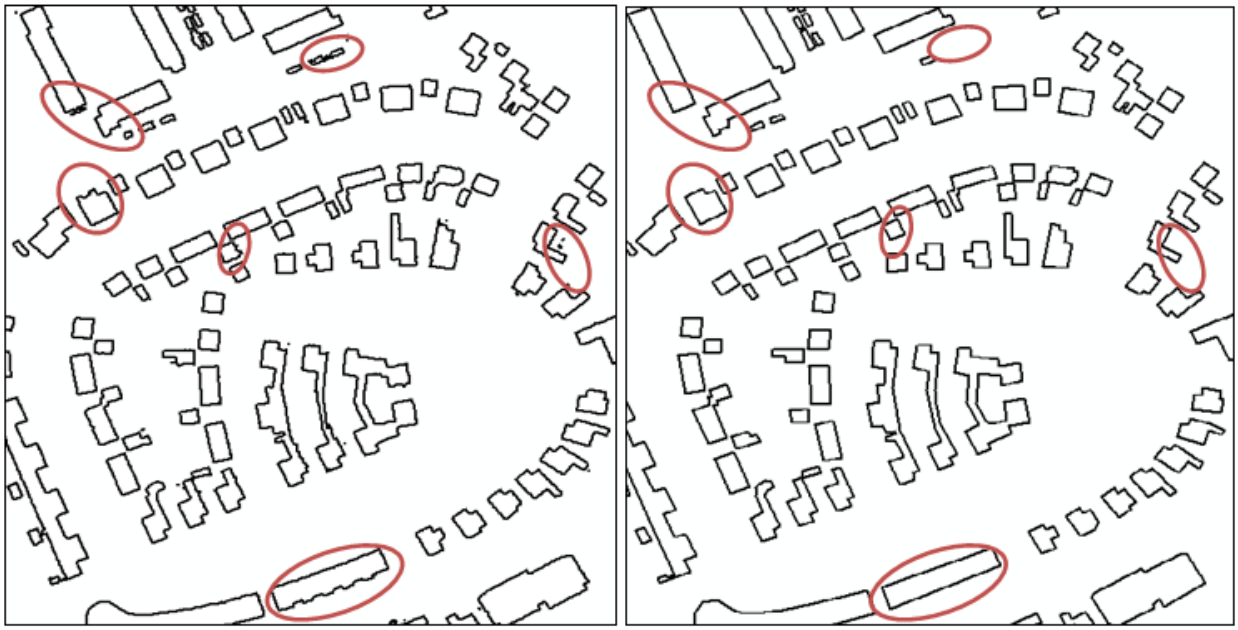

Figure 14: Initial outline before simplification (A), after simplification and removal of buildings smaller than minimum area (B)

3.2.2 RQ 2: Annual solar potential of rooftop PV

The creation of solar radiation raster data on Wageningen scale (resolution, extent) presents some challenges due to the immense size of the datasets involved. The analysis was done per 4-digit postcode area. The preparation of data is illustrated in Figure 15.

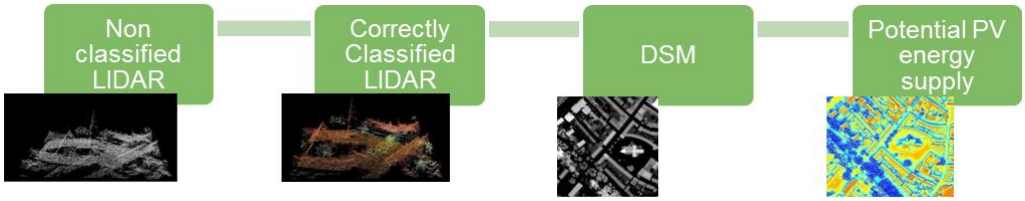

Figure 15: Scheme of LIDAR data processing

DSM interpolation

Raster, or gridded, elevation models are one of the most common GIS data types. The digital elevation model (DSM) was obtained from the LIDAR data, which provides the opportunity to make high quality elevation models. The DSM was interpolated at the resolution of 0,5 m (function LAS dataset to raster), to accurately reflect the unique characteristics of the roof, such as roof slope, roof orientation, and adjacent structures and vegetation.

DSM was obtained based on elevation. A binning technique was used to produce the raster. The MAXIMUM cell assignment type was chosen to generate DSM. In order to create a con-

tinuous surface the Void Fill method was used. The resulting DSM was interpolated at 0.5 m with natural neighbor interpolation technique.

Since roof planes with a certain angle and orientation are considered the best location for mounting a solar system, there was a need to select only roofs and trees out of DSM. Based on building outline polygons and DSM solar potential analysis was performed.

Roof solar potential estimation

In order to estimate solar radiation intensity for each cell in the selected geographical area, Area solar radiation modeling within the Solar Analyst extension, Esri's ArcGIS was used (Fu & Rich, 1999). Briefly, the model consists of three initial calculations: (i) the viewshed calculation determine which parts of the sky are obscured for every cell of DSM; (ii) the sunmaps calculations are used to estimate the amount of direct solar radiation. They identify the position of the sun based on the latitude, day of the year and time of the day; (iii) the skymaps are used to estimate the amount of diffuse solar radiation.

All initial calculations are stored as temporal two dimensional grids. Direct and diffuse radiation components are then calculated based on the amount of the sky which can be seen from each pixel (Kodysh et al. 2013).

Calculated clearness index and diffuse proportion were set according to Appendix 2. The resolution of viewshed, sunmap, and skymap were set to 200x200 cells. The number of azimuth directions used for the viewshed calculation was set to 80, which is adequate for complex topography. A skymap was divided into 8 azimuth and 8 zenith sectors and maximum sky size value was set to 400.

After the initial steps were completed, the outputs were used to calculate incoming global solar radiation (kWh/m^2). Roof slope and aspect were automatically extracted from input, which is represented by raster surface (DSM). Additional inputs were latitude of the scene center, and the date and time or specific time period for which the insolation was accumulated.

Time configuration - specifies for what period of time the solar radiation will be determined.

- *Daily interval* specifies the vertical dimension of the sectors sun maps. Calculation of direct radiation takes place after these intervals.

- *Hourly interval* specifies the horizontal dimension of the solar sector maps, which characterizes the process of calculating the direct radiation.

Since the character and amount of radiation changes over a year, the analysis was done 12 times and those monthly solar maps were added up in order to get yearly values. Daily interval for the analysis was calendar month and hour interval was set as 0,5 hour.

There is a little variation in latitude within the extent of the study area however latitude of the location was rounded up to 52. Transmissivity was set according to calculated values.

The yearly values of solar radiation represent the radiation for whole area. In order to calculate the solar radiation building roofs building outlines (BAG/LIDAR based) are used.

Actual electrical yield

The actual electrical yield depends on panel efficiency**.** Average efficiency of solar panels representing current market is 15% (Siemer & Knoll, 2013). This value is also used by Zonatlas which will be used for comparison further on in this report.
To quantify the electrical yield, annual irradiation ($kWh/m^2/year^{-1}$) was multiplied by panel efficiency and area of the cell (m^2). Invertor efficiency is neglected.

ACTUAL ELECTRICAL YIELD = ANNUAL IRRADIATION (SUM) * CELL AREA * EFFICIENCY

Suitability of roofs
Local conditions, building characteristics, weather conditions and technical parameters of solar panels give a technical potential map within Wageningen.
The categorization of suitability would be difficult with the LIDAR data only since the individual buildings are not distinguished. There is a possibility to use cadaster data for footprints of individual buildings. The categorization is derived from insolation. In this case insolation is the total amount of solar radiation energy received on a given surface (m^2) area during a given time (1 year).

Three classification methods were used for better visualization.

1. Natural breaks (Jenks) classification method was considered the most suitable because it maximizes the differences between classes and identifies the best group similar values in class (ESRI, n.d.-b).
   The generated map distinguish categories *highly suitable* roofs (dark green), *suitable* roofs (light green), *moderately suitable* roofs (yellow), *marginally suitable* roofs (orange) and *not suitable* roofs (red). Protected monuments determined by Monument Register (e.g. church, windmill, manor) were designated as *not classified* (grey).

2. The second method based on comparison of irradiation per m^2 with PVGIS based average sum of global irradiation per square meter received by the modules of the given system (kWh/m^2). Generated map distinguish building categories higher than average sum of yearly irradiation per square meter (*suitable*) and lower than average sum of yearly irradiation per square meter (*not suitable*). Protected monuments were designated as *not classified* (grey).

3. The third method calculates suitability based on maximum irradiation values in the area. Classification *suitable roofs* was assigned to roofs with at least 85% of maximum annual solar radiation in the area per building per m^2 (*green*), moderate suitable roofs was assigned to roofs with at least 70% and *not suitable* to roofs with less than 70% (see Table 4).

Table 4: Classification criteria assigning suitability classes to irradiation classes

120, 6 kWh/m^2 <	> 85% suitable	< 141,9 kWh/m^2
99,3 kWh/m^2 <	70- 85% moderate suitable	< 120,6 kWh/m^2
0,0001 kWh/m^2 <	< 70% not suitable	< 99,3 kWh/m^2

3.2.3 RQ 3: Estimation of tree shading impact on the roof-top solar potential

Since tree shading has a considerable impact on the PV electricity potential, impact of trees on solar analysis was assessed by comparing roof solar potential taking into account tree shading with roof solar potential neglecting tree shading.

Two DSMs were generated at the spatial resolution of 0,5 m. Firstly the complete LIDAR data set was used to provide information of the current urban form including both building and tree features. The second analysis utilized a LIDAR surface derived from all returns but vegetation, providing a scenario where trees shading does not affect the building roofs. In order to decrease calculation time, cells with elevation lower than 0,5m were classified as „no data“.

3.2.4 RQ 4: Determination of hot spots and cold spots

Hotspots and cold-spots (both 4-digit and 5-digit postal code based) were differentiated by subtracting electricity supply from electricity demand on a yearly basis. Since used LIDAR data are from years 2008-2012, they do not cover some newly build up parts of Wageningen.

Calculated electricity yield of buildings per 4-digit postal code areas was split into 5-digit postal code areas and a comparison with the E-atlas (Liander, 2010) was made. A table of yearly electricity consumption in households, catering and companies together in Wageningen per 5-digit postcode areas is provided in Appendix 1.

3.2.5: Validation

Quality assessment of LIDAR data was assessed by area-based accuracy measures with measures: matched overlay , area omission errors and area commission error.

The Matched overlay is computed by geometric intersection of LIDAR-based and the cadastral footprints.

Finding area omission errors the Cadaster data are considered as a reference object, LIDAR-based footprints were removed from Cadaster footprints. The total area of non-detected building parts divided by the total area of reference objects gives the percentage of non-detected footprints.

Finding area commission errors the LIDAR-based footprints were considered as reference objects and the Cadaster footprints were removed from LIDAR-based footprints. The total area of non-detected building parts divided by the total area of reference objects gives the percentage of incorrectly detected building footprints.

Randomly selected buildings were used for comparison with Zonatlas (tetraeder.solar, n.d.). Since Zonatlas uses only the most favorable parts of roofs, the yearly potential is not comparable with results of this thesis study. Validation is only done for the most favorable (parts of) roofs as used by Zonatlas. The solar potential of these selected (parts of) roofs was compared.

4 Results

This chapter illustrates the results of the previously given methodological steps. Solar potential comparing LIDAR-derived building outlines with Cadaster outlines is presented. Comparison of potential electricity yield on roofs of monuments and on roofs of other buildings is presented. Effect of vegetation shading on solar potential for a limited area is calculated and latter energy hot spots and cold spots based on 4-digit and 5-digit postcodes are described.
Lastly maps of the photovoltaic potential suitability, which can be beneficial for determining the most interesting spots for installing PV systems, are presented.

4.1 RQ 1: Roof outline footprints

Extracted roof outline polygons which were simplified in order to produce regular roof shapes and reduced to provide a profitable size of a PV system are shown in Figure 16. LIDAR-based polygons were used for comparison with cadastral outlines (see Table 7).

Figure 16: Roof outline polygons in neighborhood in Wageningen-Noordwest

4.2 RQ 2: Annual solar energy potential

Calculated atmospheric characteristics

Calculated monthly clearness index (Table 5) as well as monthly diffuse proportion (Table 6), were used for generation of solar radiation maps (Figure 17). For calculation of clearness index and diffuse proportion see chapter 3.1.3.

Clearness index varies between 0 and 1. Values 0,6 or 0,7 characterize very clear sky conditions and 0.5 generally clear sky conditions (Fu & Rich, 1999).

Table 5: Comparison of averaged monthly clearness index computed from Haarweg weather station measurements from 2008-2011

	Jan	Feb	Mar	Apr	May	Jun	Jul	Aug	Sep	Oct	Nov	Dec
Haarweg	0,303	0,301	0,415	0,512	0,482	0,467	0,441	0,426	0,425	0,411	0,286	0,277

Clearness index and diffuse proportion have an inverse relation. Diffuse proportion ranges between 0 and 1. Typical values of diffuse proportion are 0,2 for very clear sky conditions and 0,7 for very cloudy sky conditions (Fu & Rich, 1999).

Table 6: Comparison of averaged monthly diffuse proportion measured at Haarweg weather station and modeled in PVGIS.

	Jan	Feb	Mar	Apr	May	Jun	Jul	Aug	Sep	Oct	Nov	Dec
PVGIS	0.68	0.64	0.58	0.48	0.51	0.52	0.57	0.53	0.57	0.58	0.67	0.75
Haarweg	0.42	0.53	0.49	0.43	0.43	0.44	0.46	0.49	0.50	0.46	0.47	0.42

The result of the calculation for each postal code for each month is a raster representation of the geographic distribution and intensity of solar radiation on a rooftop is shown in Figure 17. It is visible that the south-facing parts of roofs result in higher potential than the north-facing parts.

Figure 17: Solar radiation estimation on roofs in neighborhood in Wageningen-Noordwest. The red color stands for the highest solar radiation intensity; blue color denotes the least solar radiation intensity and yellow is between red and blue.

LIDAR derived outlines represent the real shape and size of the roof. Both LIDAR-derived building outlines and cadaster outlines differ firstly in distinction of individual buildings as seen in Figure 18. The arrows point out examples of differences between LIDAR derived roof outlines and cadaster outlines: In case of group of buildings containing an empty space inside, only the outer boundary is extracted (marked by black arrow). Cadastral data represent ownership and dimension of the basement more than roof areas as marked by red arrow. This leads to overestimation of cadastral-based roofs. More of these characteristics are described in chapter 5 - Discussion.

A **B**

Figure 18: Solar radiation estimation on roofs in the city center. LIDAR-derived building outlines (A), cadaster outlines (B)

Potential electricity yield calculated from LIDAR-based building outlines and cadaster building outlines is shown in Table 7. Description of individual PC areas is provided in chapter 5 Discussion. The use of LIDAR based outlines results in lower output, giving more realistic figure of the potential electricity yield.

Table 7: Comparison of potential electricity yield from LIDAR-based building outlines and cadaster building outlines

Postal Code	Electricity yield cadaster (MWh)	Electricity yield LIDAR (MWh)	Difference (MWh)
6701	10 546	17 281	-6735
6702	26 497	26 699	-202
6703	13 680	20 026	-6345
6704	4 656	2 554	2102
6705	7 388	3 879	3508
6706	14 792	10 515	4277
6707	14 749	9 596	5153
6708	56 957	53 575	3382
6709	15 114	18 482	-3368
Wageningen	164 378	162 607	1772

When placing solar panels on monuments certain conditions must be met and an environmental permit (WABO) is needed (Stichting Zonne-energie Wageningen, 2013). As quantified in Table 8 and visible in Figure 19, the highest proportion of potential electricity yield generated on roofs monuments is in the city center (PC 6701). The overall proportion of electricity yield generated on roofs of monuments is negligible.

Table 8: Comparison of potential electricity yield on roofs of monuments and on roofs of building

Postal Code	Electricity yield (MWh)	El. yield buildings (MWh)	El. yield monuments (MWh)	El. yield of monuments [%]
6701	10 546	9 808	738	7,0
6702	26 497	26 400	97	0,4
6703	13 680	13 345	335	2,4
6704	4 656	4 656	-	0,0
6705	7 388	7 320	68	0,9
6706	14 792	14 788	4	0,0
6707	14 749	14 709	40	0,3
6708	56 957	56 923	33	0,1
6709	15 114	15 114	-	0,0
Wageningen	164 378	163 063	1 315	0,8

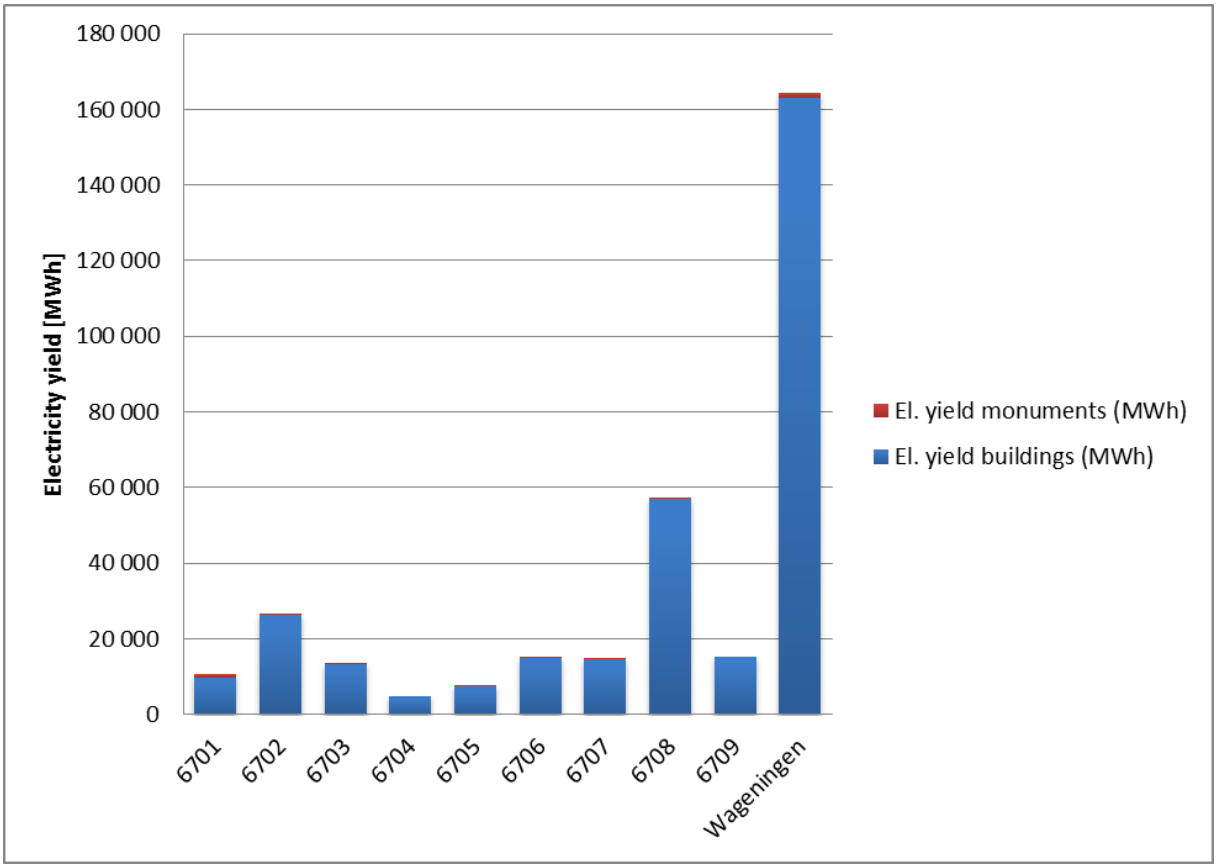

Figure 19: Proportion of potential electricity yield on monuments

Electricity yield scenarios

For installation of solar panels, roof space with optimal conditions is preferred. Because of small structures on the roofs (chimneys, dormers etc.) and poor conditions roof surfaces must be reduced. Thus realistic assumption of a roof area suitable for PV installation can be estimated as 75% of the roof. Different scenarios of 100% and 75% suitable roof area in relation to high performance PV panels (20% efficiency) and average conventional panels (15% efficiency) were made. Those four scenarios were compared with electricity consumption of PC 6708 which represents the largest 4-coded post code area (see Figure 20).

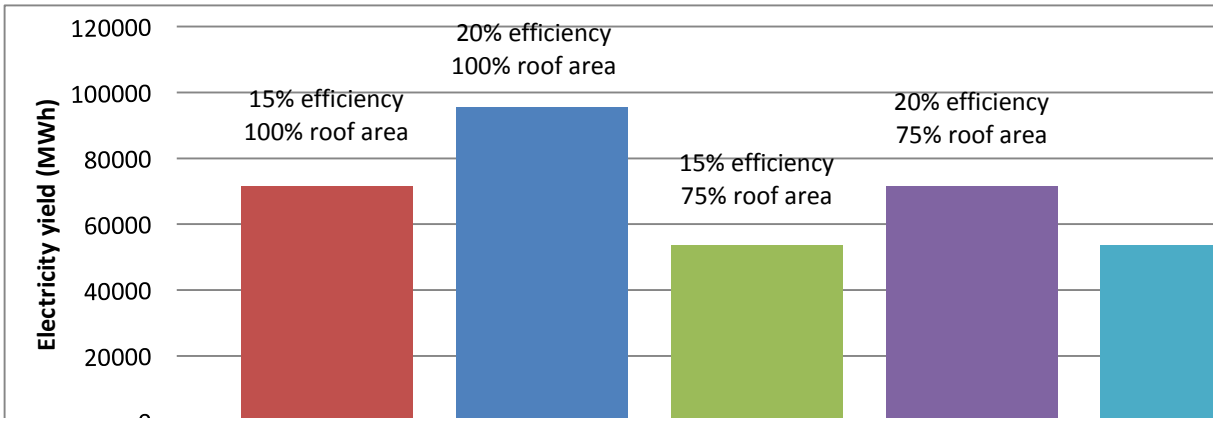

Figure 20: Different scenarios of potential electricity yield calculated for PC 6708 taking into account roof area reduction and high performance PV panels

High performance panels with reduced roof area can compensate the reduction of roof area. Even with 75% of roof space PC 6708 would generate enough electricity (53 641 MWh) to meet its annual electricity demand (53 575 MWh).

4.3 RQ 3: Estimation of tree shading impact on the roof-top solar potential

The difference in solar radiation values between the not shaded part of the roof and shaded parts of the roofs is visible in Figure 21. The arrow points to part of the roof which is not shaded by adjacent trees (A), and part of roof affected by tree shading (B)

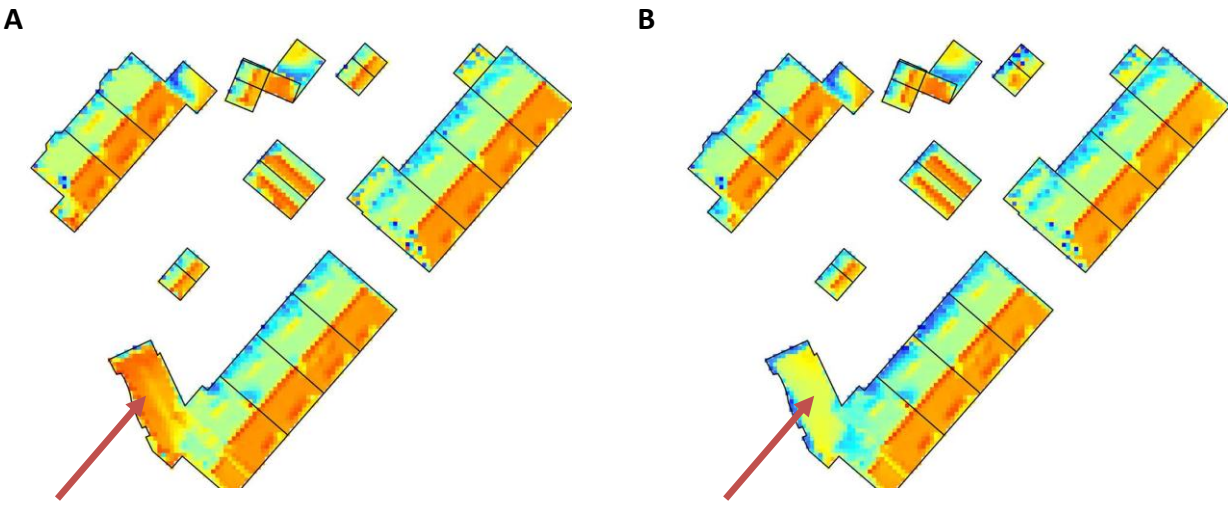

Figure 21: PV roof top potential without trees shading (A), PV roof top potential with trees shading (B)

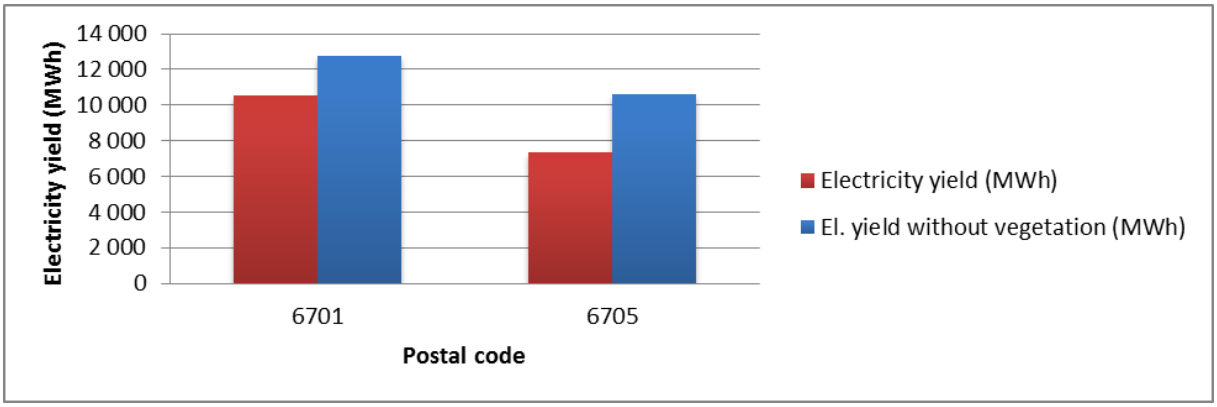

Figure 22: Impact of vegetation influence on electricity yield in less vegetated area (PC 6701) and area with a lot of vegetation (PC 6705)

Trees can limit solar access on roofs where solar panels can be installed. Impact of vegetation influence on electricity yield was estimated for two different 4-digit PC areas: less vegetated area represented by city center (PC 6701) and area with a lot of vegetation represented by residential area (PC 6705). In this calculation 100% stands for the electricity supply with tree shading. In case of neglecting of vegetation influence, electricity yield would increase by 21% in PC 6701 and by 43,5% in PC 6705 as visible in Figure 22 and Table 9. Calculated impact of vegetation influence on electricity yield can be considered in future tree planting.

Table 9: Electricity yield gain without vegetation influence in less vegetated area (PC 6701) and area with a lot of vegetation (PC 6705)

Postal code	6701	6705
Electricity yield (MWh)	10 546	7 388
El. yield without vegetation (MWh)	12 763	10 600
El. yield gain without vegetation influence [%]	121	143

4.4 RQ 4: Hot and cold spots and self-sufficiency

Energy hot spots and cold spots on the potential energy supply and demand were found on a 4 digit postcode area (see Table 10 and Figure 23) and 5 digit postcode area (see Appendix 3). Yearly electricity supply of whole Wageningen covers 98,9% of its electricity demand (see Figure 23).

Table 10: Energy hot spots and cold spots based on 4-digit postcodes and solar potential calculated from real DSM

Postal Code	Electricity supply (MWh)	Electricity demand (MWh)	Hot spot (+)/cold spot (-) (MWh)
6701	10 546	17 281	-6735
6702	26 497	26 699	-202
6703	13 680	20 026	-6345
6704	4 656	2 554	2102
6705	7 388	3 879	3508
6706	14 792	10 515	4277
6707	14 749	9 596	5153
6708	56 957	53 575	3382
6709	15 114	18 482	-3368
Wageningen	164 378	162 607	1772

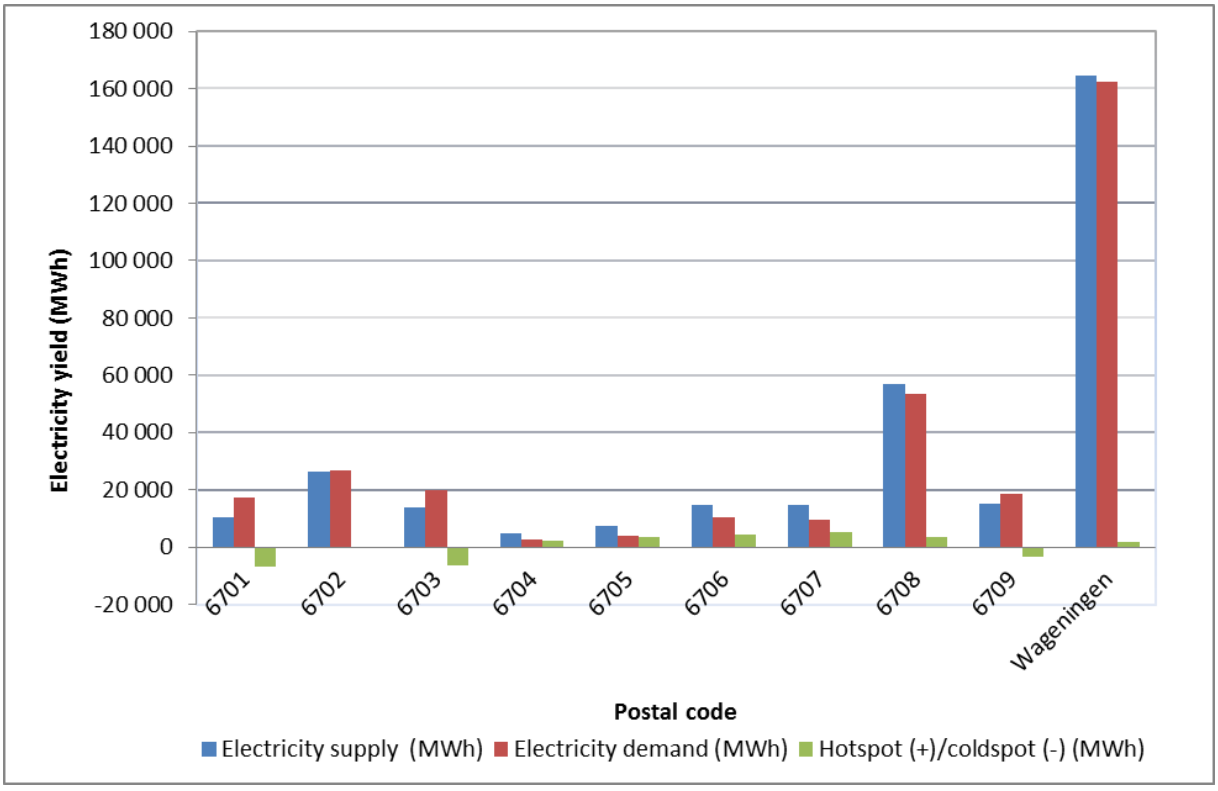

Figure 23: Energy hot spots and cold spots based on 4-digit postcodes

Electricity hot spots and electricity cold spots indicate where yearly potential electricity supply exceeds the electricity demand and demand exceeds the potential electricity supply respectively (see Figure 24-Figure 26).

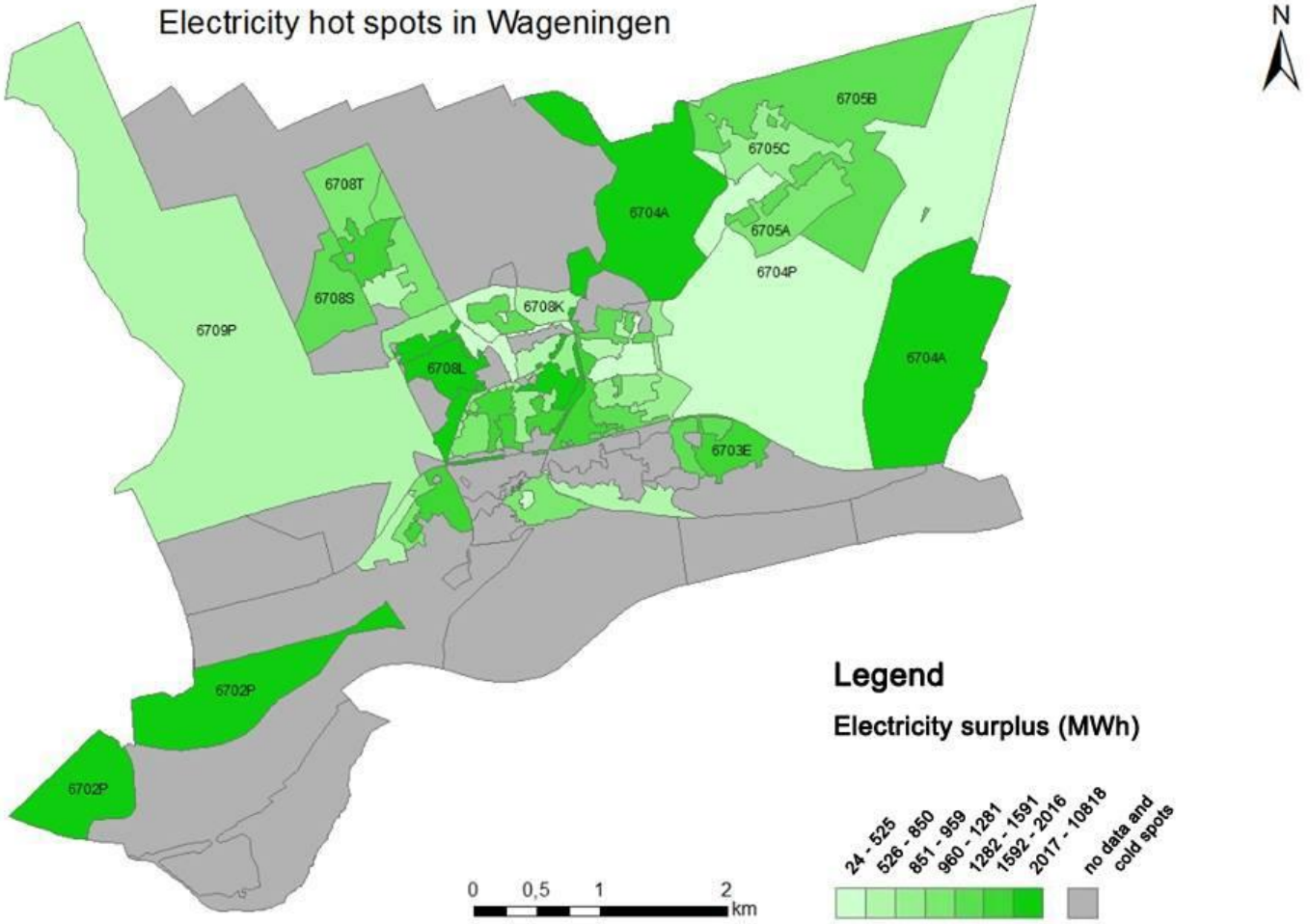

Figure 24: Electricity hot spot based on 5-coded postal code areas

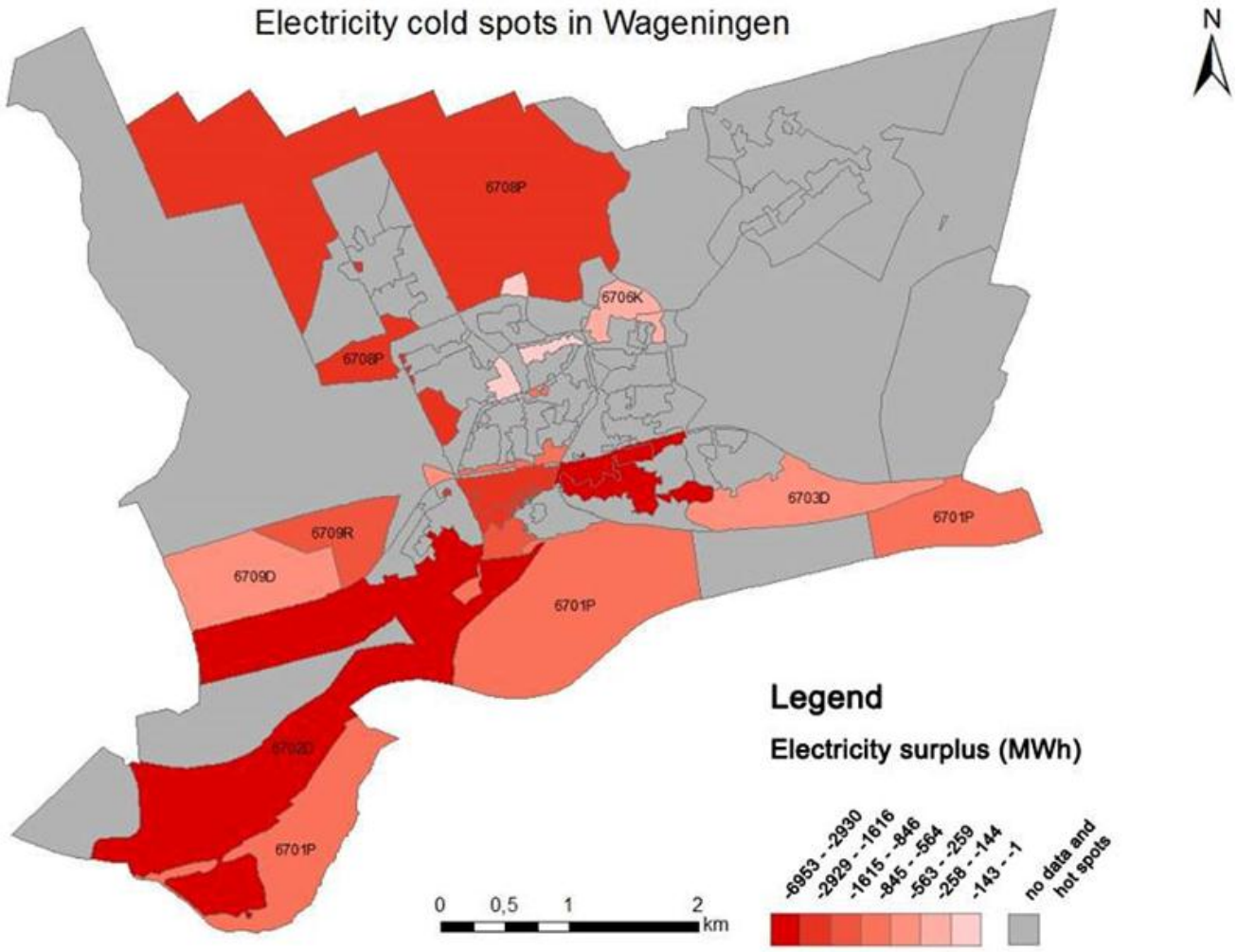

Figure 25: Electricity cold spots based on 5-coded postal code areas

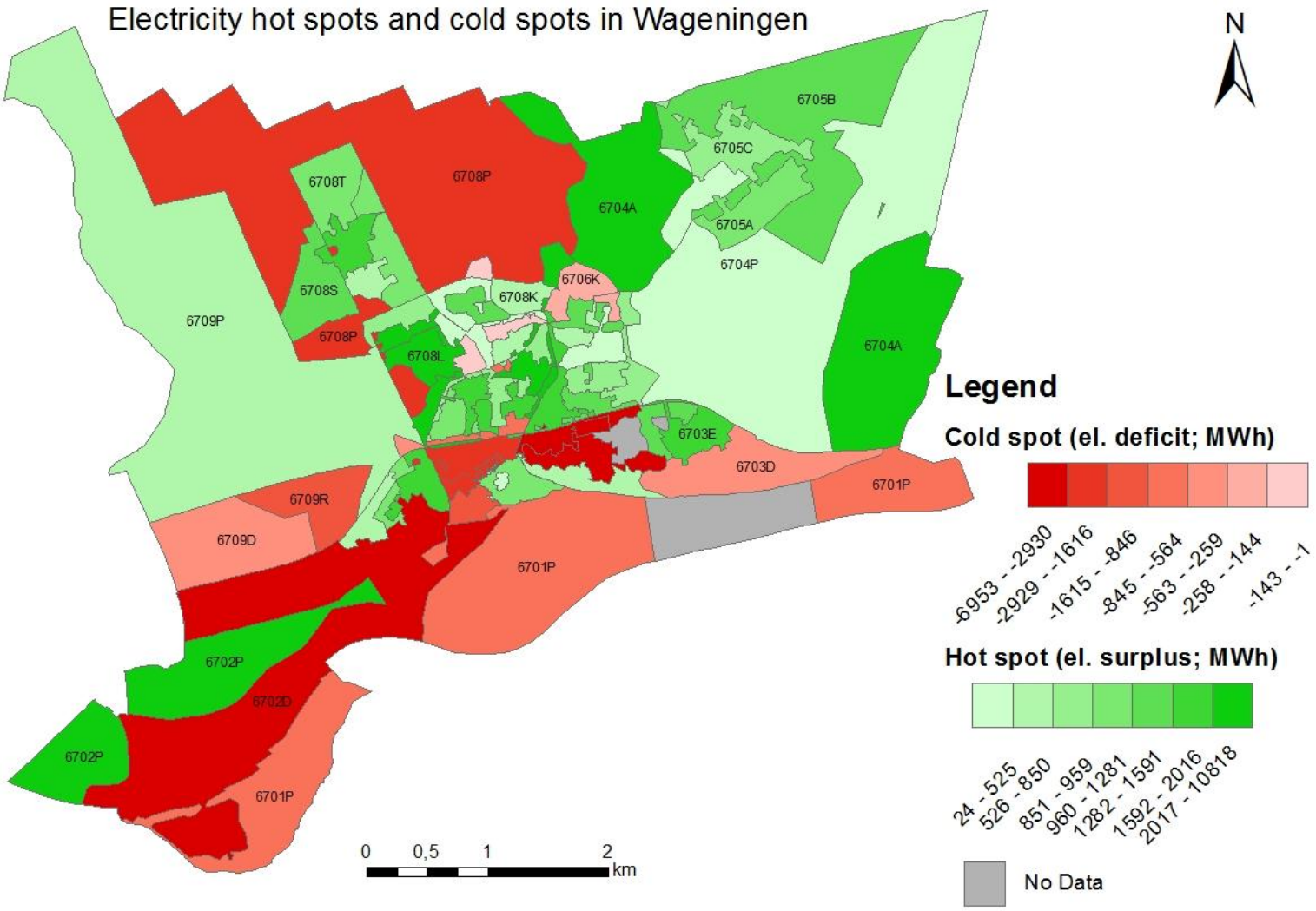

Figure 26: Electricity hot spots and cold spots based on 5-coded postal code areas

Hot-spots and cold-spots provide interesting subject for discussion. As the composition of individual postcode areas differ, short description of postcode areas and interesting 5-digit postcode areas are mentioned below (in postcode areas where 4-digit PC and 5-digit PC match). As Wageningen has got different buildings and usages some conclusions will be drawn of those.

6701

The PC 6701 represents the city center of Wageningen and area connecting the city center and the river Rhine. In this area electricity demand is higher than potential supply.

6702

PC 6702 is a part of Wageningen consisting mainly of blocks buildings and buildings representing trade, crafts and industry. Electricity demand is slightly higher than potential electricity supply as Nude Park is a large consumer of energy.

6703

Number of villas, arboretum and old university campus are situated in PC 6703. Electricity demand exceeds potential electricity supply.

6703H was missing in the E-atlas.

6704

PC 6704 represents area with houses and villas scattered in forest. Despite influence of vegetation, supply is higher than demand.

6705

PC 6705 represents similar area as PC 6704. Supply exceeds the demand. Typical examples of those 5-digit PC are: 6705A, 6705C, 6705 D.

6706

PC 6706 comprises of block buildings, university buildings and family houses. Potential electricity supply exceeds electricity demand. Typical examples of 5- digit PC are: 6706E, 6706G, 6705J.

6707

PC 6707 represents block buildings and semi-detached houses. In this area potential electricity supply is higher than electricity demand. Typical examples of 5- digit PC are 6707B, 6707D, 6707J.

6708

PC 6708 comprises of block buildings, semi-detached buildings, detached buildings and university campus. Electricity generated by solar panels would be higher than el. demand.

6708R representing flats, as well as 6708C representing area with semi-detached houses with higher potential electricity supply than demand. On the contrary 6708P representing a site where most of the buildings of Wageningen University used for both research and educational purposes are situated has dramatically higher consumption than potential electricity yield.

6709

PC 6709 comprises of student housing complexes, educational buildings, and commercial buildings. Electricity demand in this area is higher than potential electricity supply.

On the contrary in 6709P representing commercial and educational buildings and part of student housing potential electricity yield is substantially higher then electricity consumption.

As large energy consumers such as university or industry buildings consume more energy than possible production and they have cheaper electricity due to better tariffs, there would not be a financial incentive to install solar panels on their roofs. On the contrary small energy consumers such as residential buildings are more prone to install solar panels on their roofs as their electricity tariffs are high.

Based on the evaluated potential 5- digit postcodes are colored according to their potential self-sufficiency (Figure 27). Considerable proportion of Wageningen is classified as self-sufficient or nearly self-sufficient.

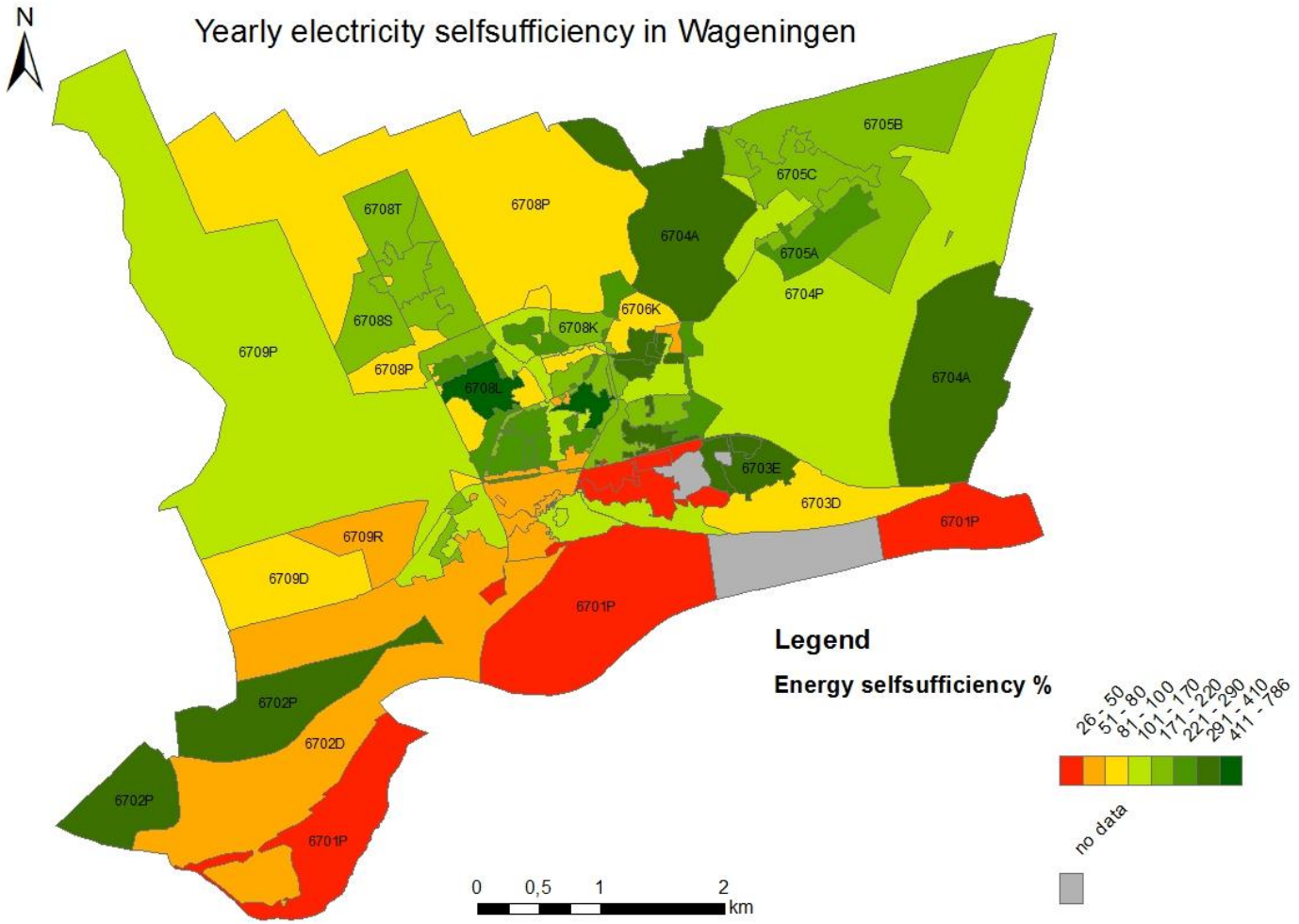

Figure 27: Electricity self-sufficiency based on 5- digit postcodes in Wageningen

4.5 Suitability maps

Four different parts of Wageningen were used for visual comparison and suitability maps were created (see Figure 28-Figure 30). Three different ways of classification were chosen as classification influences perception of results. Their description can be found in section 3.1.5.

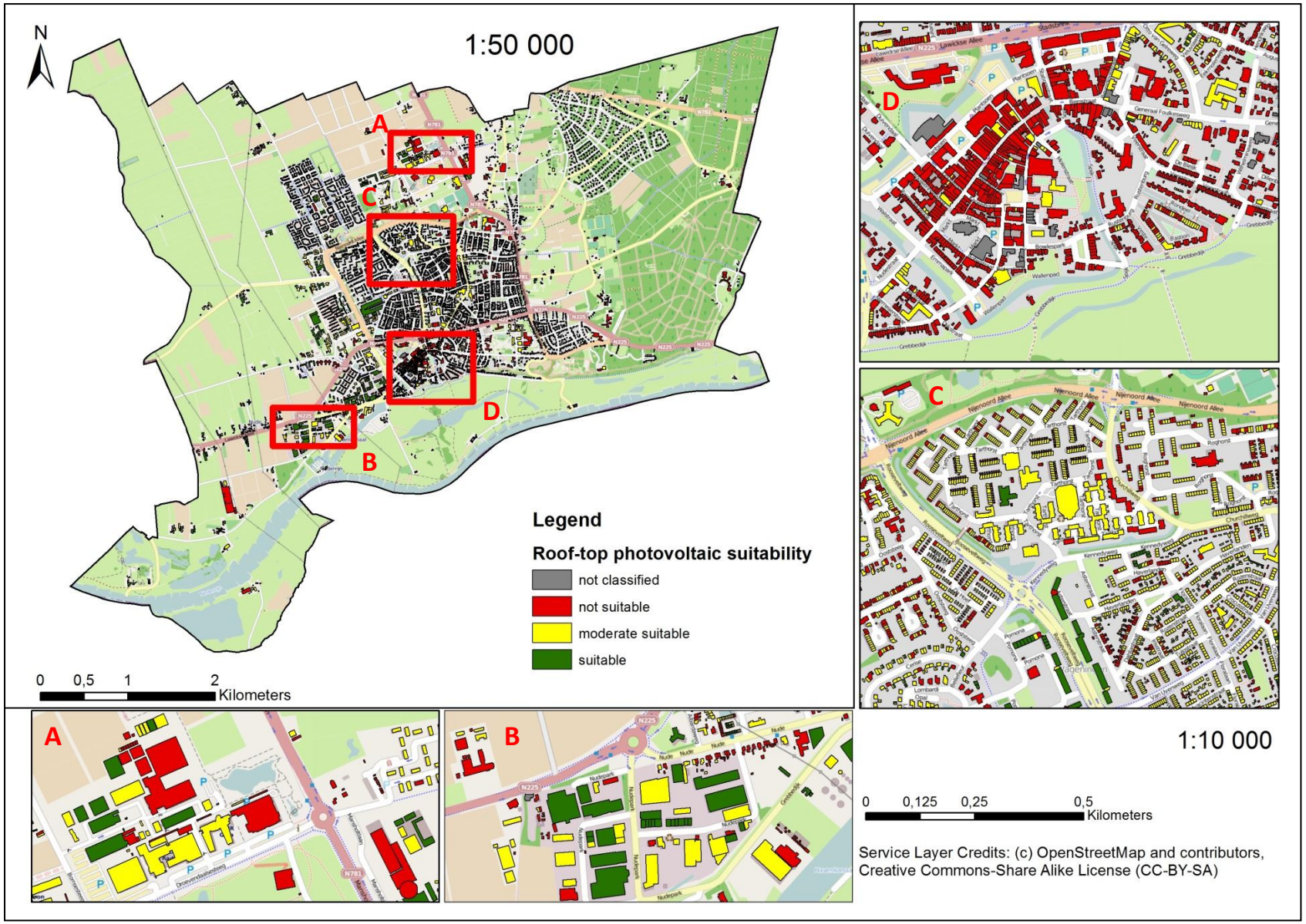

Figure 28: Suitability map of Wageningen based on maximum irradiation values in the area. A – part of campus, B – Nude park, C – family houses neighborhood, D – city center

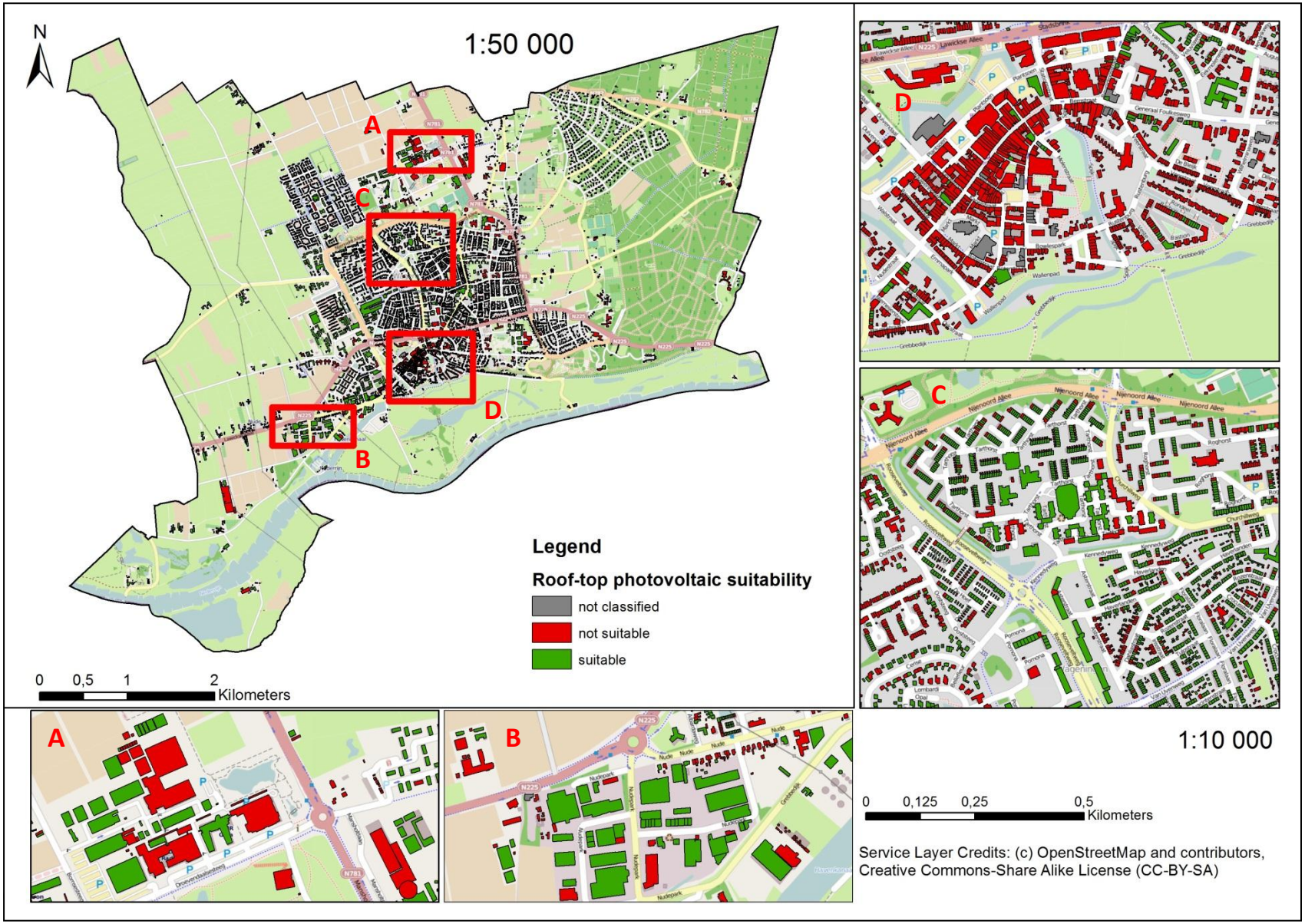

Figure 29: Suitability map of Wageningen based on comparison with PVGIS based average sum of global irradiation. A – part of campus, B – Nude park, C – family houses neighborhood, D – city center

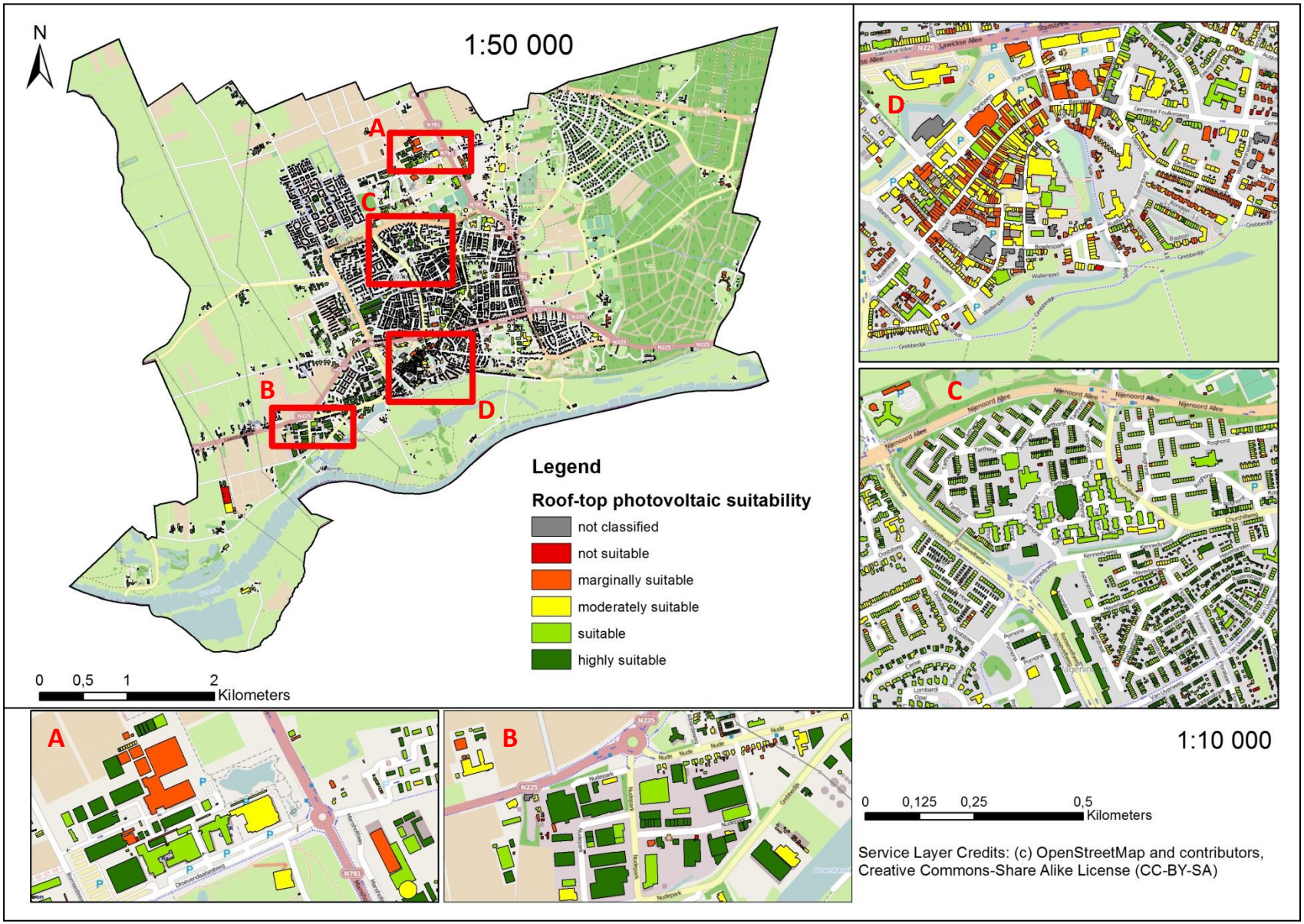

Figure 30: Suitability map of Wageningen based on Natural breaks (Jenks) classification. A – part of campus, B – Nude park, C – family houses neighborhood, D – city center

Out of all selected areas which represent WUR campus, Nude Park, residential area and city center it is obvious that Wageningen city center (D) where most of the shops and restaurants are located is not favorable for siting of PV panels. On the other hand Nude Park (B) and family houses neighborhood (C) are one of the most favorable.

Suitability classification based on maximum irradiation values it is considered the most relevant as it represents an adapted classification of Zonatlas (tetraeder.solar, n.d.). As visible in Figure 31 only 17% (~291 000 m^2) of roofs in Wageningen are classified as suitable. On the other hand the moderate suitability and unsuitability account for the majority 36% (~599 000 m2), 46% (~765 000 m2) respectively. Only 1% of all roofs in Wageningen were not classified because they were considered monuments.

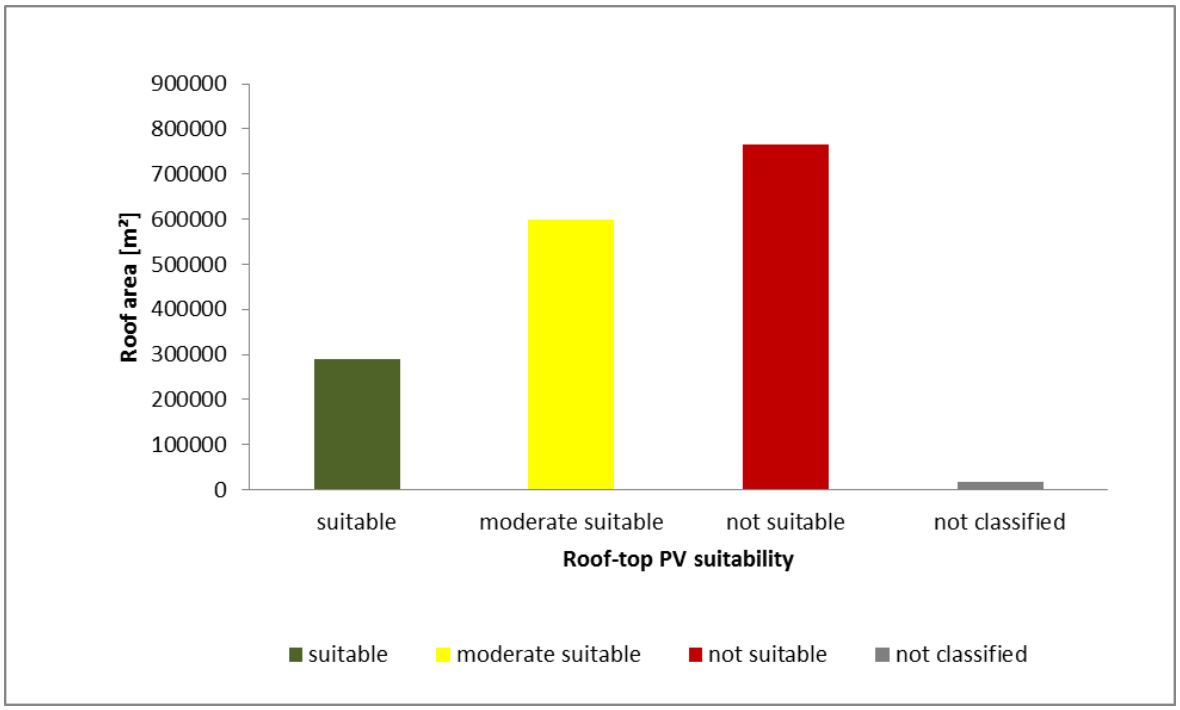

Figure 31: Suitability based on irradiation values in area

The comparison with the PVGIS based average sum of global irradiation states whether a building has a higher irradiation than the average per m^2 (suitable), or lower irradiation than the average per m^2 (unsuitable). According to the PVGIS based criteria, 95% (~840000m^2) of all roof surfaces are classified as not suitable as visible in Figure 32.

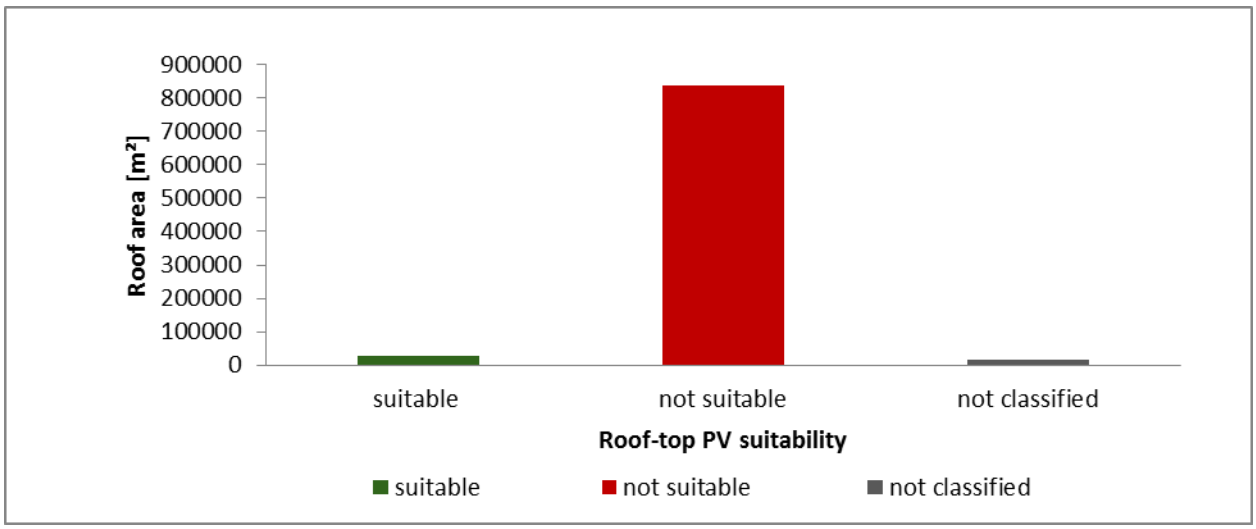

Figure 32: Suitability classes based on PVGIS

Whereas suitability classifications based on maximum irradiation values and Natural breaks (Jenks) classification speak in favor of solar panel installations, PVGIS based classification gives restrictive results. The 5% of suitable roofs of this classification can therefore offer the most suitable roofs from a cost performance analysis. Monuments stand for only 1 percent of all roof surfaces thus installation of solar panels on roofs of monuments is insignificant.

5 Validation

Three levels of evaluation to test the precision of the method were used. Firstly used solar radiation tool and atmospheric data were validated, secondly LIDAR based building footprints and at the end the potential electricity yield.

Validation of the tool and atmospheric data

Figure 33 represents graph comparing the computed yearly insolation for site of former weather station, Haarweg in kWh/m^2 (Model I) with pyranometer data from Haarweg weather station and PV GIS - Solar Radiation Atlas. The result shows that our used method underestimates the insolation in winter months.

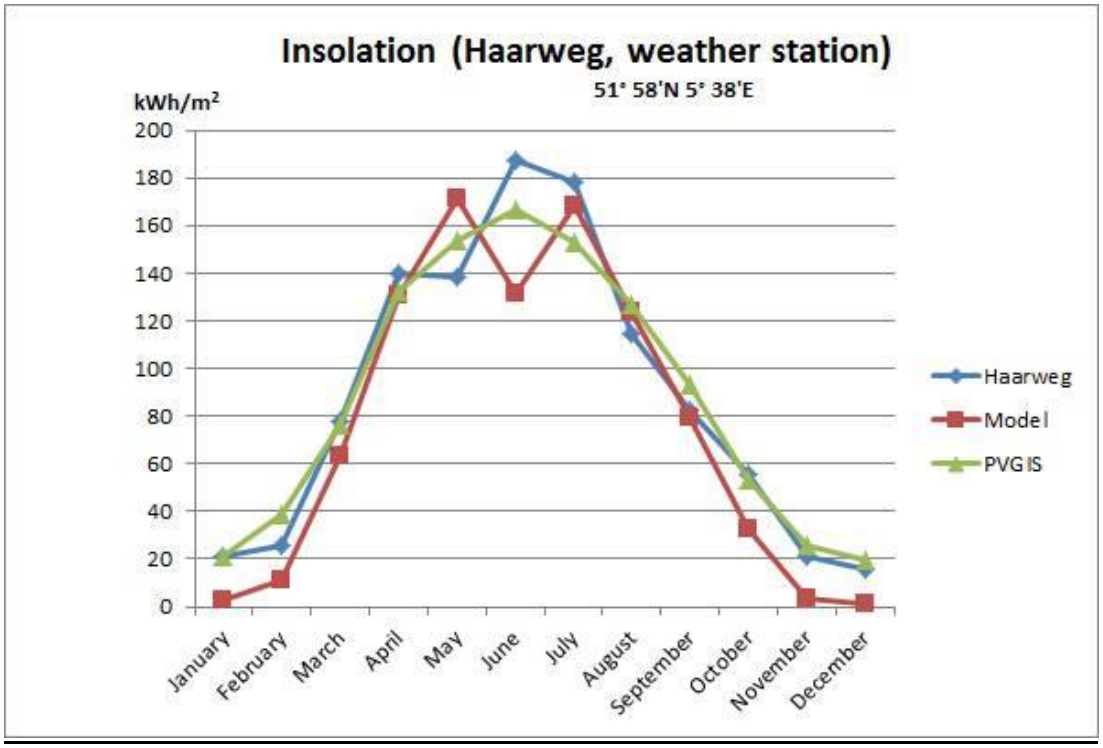

Figure 33: insolation values over a year in Haarweg weather station

Available roof surface comparison

The total area of all LIDAR based roof footprints and cadaster footprints in Wageningen was evaluated. Correctness verification of LIDAR data was performed based on (Song & Haithcoat, 2005). Cadaster data are considered „true“ reference.

Matched overlay which stands for the percentage of overlapping parts of reconstructed buildings to the total area of reference building regions is 82%.

Area omission errors which stands for total area of non-detected building parts divided by the total area of reference objects is 13%.

Area commission error which stand for total area of incorrectly detected building parts divided by the total area of detected objects is 10%.

These errors are caused by different reasons. Cadastral data could be outdated (not matching with LIDAR). Buildings with glass exteriors generate noise and does not provide a detectable return from these surfaces were omitted. Small buildings such as bike sheds, terraces and balconies are not suitable for PV installation, therefore they were not used.

Roof areas of following buildings were compared with the roof surfaces in thesis from Wolf Bierens (Table 11). Surfaces in his study were calculated by the measurement tool of Google maps.

Table 11: Overview of roof areas of selected buildings. Comparison with data of Bierens, 2013

	Vada graphic	Technotron	Marin	Haverlanden	Haarweg
Whole roof surface cadaster based [m2]	4 951	2 821	27 538	7 711	6 725
Whole roof surface LIDAR based [m2]	4 925	3 026	28 383	8 035	6 798
Net PV Surface (Bierens, 2013)	**3 000**	**1 500**	**18 000**	**2 378**	**1 500**
Bruto surface (Bierens, 2013)	**4 230**	**2 115**	**25 380**	**2 378**	**2 115**

The area of LIDAR based roof surfaces and cadaster based roof surfaces provide comparable data (Table 11). However in comparison with Bierens (2013) there is an overestimation of roof areas. The roof surfaces of Vada graphic and Technotron are comparable whereas roof surfaces of Haverlanden and Haarweg differ substantially. The decrease of roof areas in Bierens (2013) is caused by reduction to only south facing roofs in case of Haverlanden and use of only the upper terraces in Haarweg. For this reason calculated building production are not comparable either.

Comparison of electricity yield

Likewise calculated electricity yield of those buildings was compared with results of Bierens (2013) (Table 12) while overestimation of roof surfaces is taken into account. As potential electricity yield is derived from the roof surface, Haverlanden and Haarweg provide incomparable results as Bierens (2013) considered only south facing roofs, however large flat buildings (e.g. Vada graphic) provide comparable results.

Table 12: Overview of annual electricity consumption and annual production of selected buildings. Comparison of two scenarios with data of Bierens (2013)

	Haarweg	Haverlanden	Vada Graphic	Marin	Technotron
Annual Consumption	1311 MWh	431 MWh	650 MWh	3127 MWh	756 MWh
Annual Production Scenario (14.2%) (Bierens, 2013)	87 MWh	317 MWh	173 MWh	1021 MWh	85 MWh
Annual Production Scenario (20%) (Bierens, 2013)	276 MWh	443 MWh	552 MWh	3314 MWh	275 MWh
Annual Production LIDAR based (15%)	633 MWh	860 MWh	628 MWh	3549 MWh	331 MWh
Annual Production LIDAR based (15%) 75% roof area	475 MWh	645 MWh	471 MWh	2662 MWh	248 MWh

Annual electricity production of Technotron was estimated for four scenarios (see section 4.3) comparing LIDAR-based and cadaster based outlines (see Table 13). For comparison with Bierens (2013) see Table 11.

Table 13: Overview of calculated annual electricity potential of Technotron. Comparison of LIDAR based and cadaster-based data and different scenarios

Technotron	Annual production	
Scenario	LIDAR - based	cadaster - based
15% panel efficiency; 100% roof area	331 MWh	319 MWh
20% panel efficiency; 100% roof area	442 MWh	425 MWh
15% panel efficiency ; 75% roof area	248 MWh	239 MWh
20% panel efficiency; 75% roof area	331 MWh	319 MWh

Zonatlas is an interactive tool providing information about suitability of the roof areas for generation of solar energy. The potential electricity yield is counting with panel efficiency factor of 15%.

Randomly selected buildings were used for comparison with Zonatlas (Figure 34). Since Zonatlas uses only the most favorable parts of roofs (Figure 35), calculated yearly potential of those parts could be compared with Zonatlas.

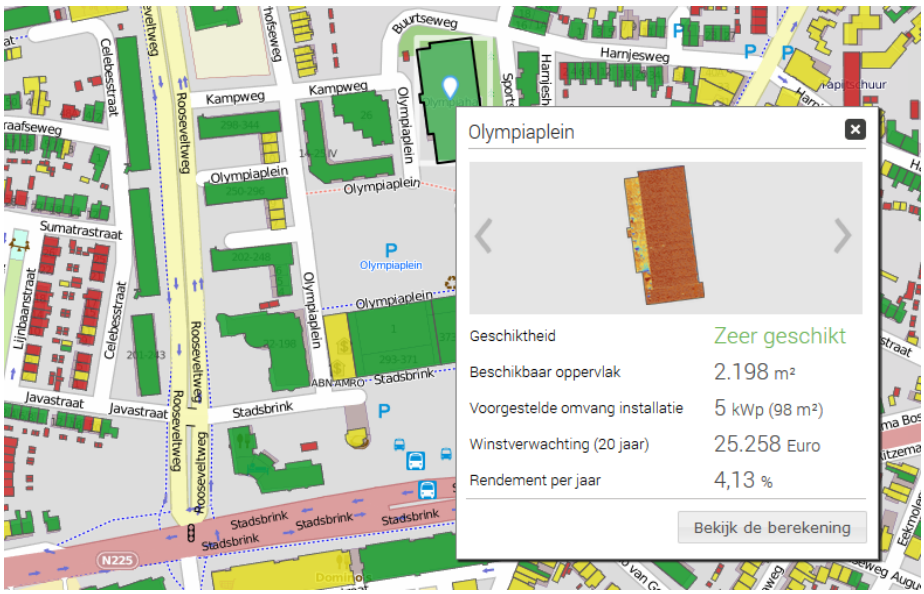

Figure 34: Screen shot Zonatlas Gelderland with PV details regarding roof suitability for PV installation

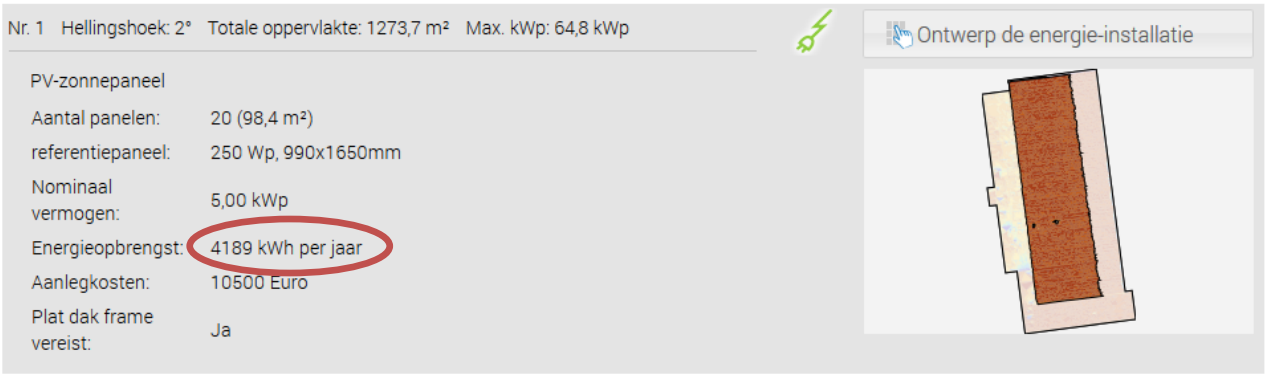

Figure 35: Screen shot Zonatlas: Building ID 947468 - roof with the most return for solar panels

As seen in Figure 36 the calculated electricity yield calculated for pitched roofs is comparable with Zonatlas values. A table with comparison of roof areas and potential electricity yield is available in Appendix 4.

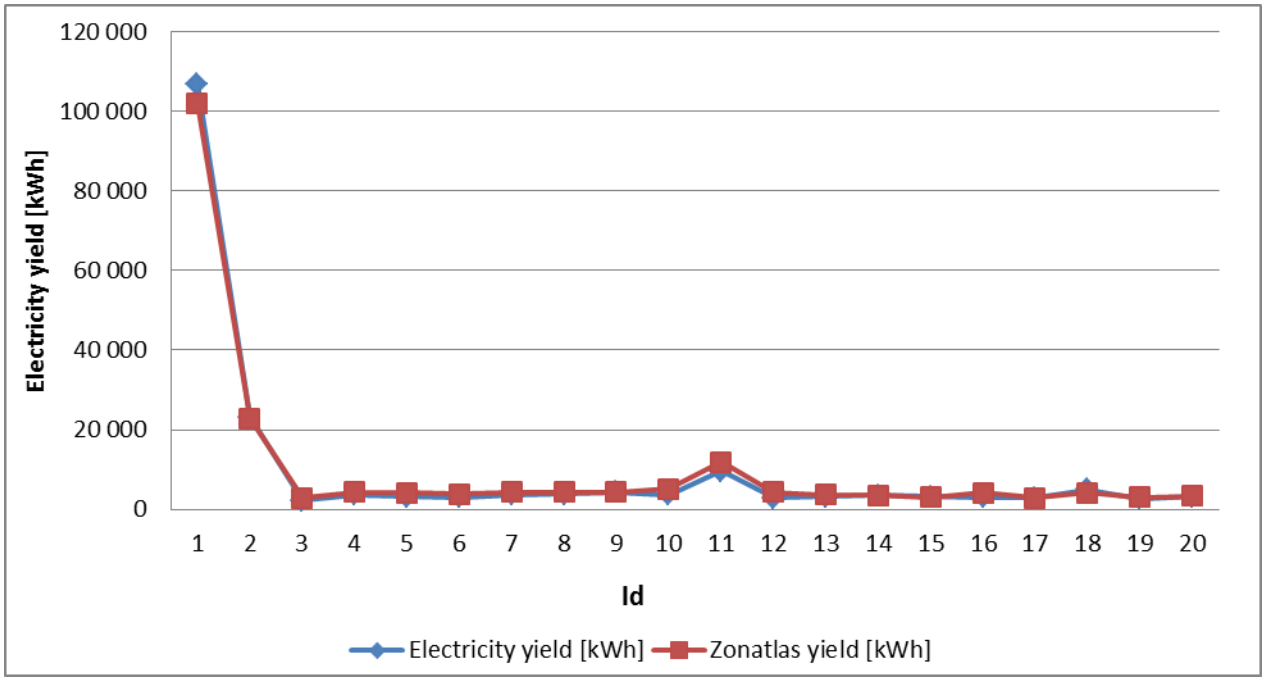

Figure 36: Comparison of calculated electricity yield on gable roofs with Zonatlas values

A table with comparison of roof areas and potential electricity yield available in Appendix 4. For flat roofs the result differs substantially as seen in Appendix 4 and calculated electricity yield is systematically higher than the Zonatlas based (Figure 37). For smaller roofs the difference in potential electricity yield is not visible however with growing size of flat roof the calculated potential electricity yield makes a big difference.

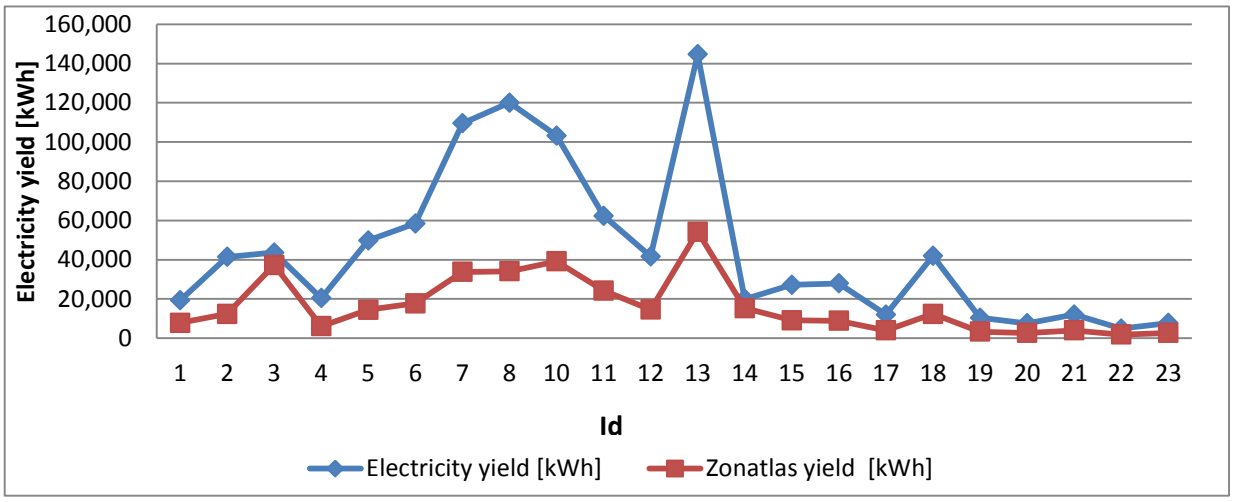

Figure 37: Comparison of calculated electricity yield on flat roofs with Zonatlas values

6 Discussion

In this chapter different aspect of this study are critically reviewed. This section discusses the input data and spatial resolution (6.1), selected parameters (6.2), followed by data processing and results of each RQ (6.1-6.6).

Assumptions

Following assumptions were made.

- It is assumed the efficiency and temperature are constant and there is no threshold above which the panels start producing electricity and no saturation problems occur.
- The monument dataset containing church, wind mill, manor and other historical buildings was used as a representation of unsuitable buildings and therefore excluded from final electricity yield potential.

6.1 General discussion

Input data

Even though I used LIDAR data with high point density, in some places the points (in a cloud) are missing, which causes the holes in LIDAR-derived building polygons. These poor results are caused by highly reflective surfaces like glass or tree occlusion.

Data from different years were used in this research. Since LIDAR scanning of Wageningen took place in 2010 and electricity demand data are from 2008, there was an effort to match the BAG data and post code data with it. Due to outdated LIDAR data, newly build up and demolished buildings are not covered in the analysis. Not matching data apply also for postcodes: 4-digit PC from year 2008 and 5-digit PC from year 2006. Discrepancy in used data has to be considered in future use.

Spatial resolution

As seen in Table 2 the resolution used in existing studies ranges from 0,55m up to 200m x 200m. According to data accuracy and extent of study area I consider resolution 0,5m appropriate. Coarser resolution could be used for the whole Wageningen however it would probably lead to less accurate results of solar analysis. Finer resolution would increase the processing time signifi-cantly.

6.2 Selected parameters

Atmospheric conditions were taken into account with use of *diffuse proportion factor* and *clearness index* I calculated.
Some important factors were not included because of missing data. As mentioned in the chapter "*Parameters selection*", temperature should be taken into account for those situations above 25 degrees Celsius, since it is the cell efficiency dropping threshold. Roofs can heat up to ~45-55 degrees Celsius (Kruza, 2011), however temperature data of individual roofs is not available. Therefore this parameter is neglected. Exposure to humidity which influences the PV cell's performance negatively is neglected for the same reasons as roof temperature (but see Mekhilef et al., 2012).

6.3 LIDAR data processing and building footprints

Different sources consider outline of the buildings differently – number of sources describe the walls of a building as the footprint while other consider roof outlines the footprint of a building. In this case building footprints were obtained with use of LAStools from manually reclassified LIDAR data in a way they represent rooftop outline. Cadastral outlines were used for comparison as they represent the only official and available data source providing building outlines. These data however do not always represent the shape and size of a rooftop. Both cadastral data and LIDAR-derived outlines have its advantages and disadvantages, which are listed in Table 14.

Table 14: Comparison of cadaster (BAG) outlines and LIDAR-derived building outlines

Cadaster	LIDAR-derived outlines
Distinction of individual buildings	No distinction of individual buildings
Representation of ownership and dimension of basement	Real shape and size of roof
- straight outlines	- dependent on LIDAR data quality - not appealing, simplification/regularization needed

- Comparison of potential electricity yield from LIDAR-based building outlines and BAG building outlines in Table 7 shown that cadastral data are overestimated.
- Zonal statistics cannot handle overlapping objects therefore fully overlapping objects were discarded (see Table 15). In case of partial overlap, zonal statistics (SUM) is calculated for the higher objects and for the not overlapping part of lower object. The fact that there are fully overlapping objects might limit the use of cadaster data for such purposes without proper data adjustment.

Table 15: Overlapping buildings from cadaster (BAG) data

Postal code	number of overlapping buildings
6701	1
6702	0
6703	4
6704	1
6705	0
6706	23
6707	14
6708	4
6709	1

6.4 Annual solar potential

Due to limited computation memory it was not possible to create TIN through LAS to multipoint for some 4-coded postal code areas, therefore the methodology had to be altered.

Solar Analyst is one of the most popular tools to calculate solar potential however it does not take into account reflections between buildings, from surrounding trees or from the urban terrain. As Jakubiec & Reinhart criticized use of constant values of sky transmissivity and the ratio between direct and diffuse insolation throughout the year, these values were calculated per individual months.

Solar cell potential

Number of directions around a location of interest used in viewshed calculation can have a significant impact on solar potential calculation. When deciding which number of directions to choose, it is necessary to consider what the nature of the surface area is. Since DEM of area of interest contains both buildings and vegetation, I chose the maximum number - i.e. 80 directions. For example, in case of small number of directions some shading obstacles may be excluded from calculations. With raised number of directions the calculation time increased significantly.

The maximum sky size value ranges up to 4000. The smaller the day interval, the higher the sky size value recommended. In this analysis sky size was set to 400 in order to avoid rapid increase of calculation time.

Calculation time

Solar radiation calculation is computationally demanding and it would not be possible to run it for entire Wageningen at once. Calculation time is depending on area and individual computer. Division of the DEM must be done in a way to have smallest impact on the final result due to shading. It was necessary to pay attention to separation of elements which can possibly shade each other.

The analyzed area has been divided into 9 sectors according to the 4-coded zip codes. The processing was realized for each month individually by using 12 models running on 12 computers. The approximate calculation times (median) per each month are stated in following Table 16, however it was not an exception that on some computers the calculation time was twice or three times as longer. This can be explained by possible differences in computer hardware.

Table 16: Solar analysis calculation time per month

Postal code	Calculation length
6701	5 hours
6702	26 hours
6703	13 hours
6704	46 hours
6705	6,5 hours
6706	1,5 hours
6707	1 hour
6708	41 hours
6709	46 hours

Size limitations

In principle there is no limitation to the size of a PV-installation, however the PV-panels should be installed in such a way that they are cost-effective. With increasing size of the PV system, the unit cost per Watt decreases. Although authors define a minimum system size of 15 m^2 (Ludwig, Lanig, & Klärle, 2009) or 20m^2 (Carneiro, Morello, & Desthieux, 2009), most of the studies consider roof size 10 m^2 as a minimum (Bergamasco & Asinari, 2011; Brito, Gomes, Santos, & Tenedório, 2012; Highman, 2011; Hofierka & Kaňuk, 2009; Santos et al., 2011).
This threshold was used both due to economic reasons and to time demanding point cloud classification.

Interpretation
In order to visually aid decisions regarding energy planning and avoid misinterpretation, I adapted classification of Zonatlas to three classification maps using different categories. These maps are showing a suitability of roofs for solar panel installation.

Overestimation and underestimation of solar potential
Roof features such as skylights or pre-existing solar systems were neglected. That means that existing roof elements were also accounted for in the available solar area therefore area available for

solar panels was overestimated. Reflected radiation from surrounding trees and buildings was not taken into account.

Validation
The average electricity yield in Wageningen is about 140-150 kWh/m^2 per year. Zonatlas results does not match with this assumption as seen in example Figure 35, moreover their calculated electricity yield does not change with increasing roof area (see Appendix 4).

6.5 Tree shading

Impact of tree shading depends on seasonality. The AHN-2 laser scanning of Wageningen took place in early spring when there had nearly no leafs. That means that laser beams were reflected by tree trunks and branches. LIDAR-derived tree heights tend to be underestimated, especially when data are collected in leaf-off period. Therefore the calculated influence represents the scenario when the influence of tree shading should be at its minimum. However I assume that at DSM resolution of 0.5 x 0.5 m the difference between leaf-off and leaf-on period is negligible. The distinction of deciduous and coniferous trees which do not change seasonally is neglected. Due to its rare occurrence trees intervening above trees are neglected.

Due to demanding computation power analyses the estimation of tree shading impact on the rooftop solar potential was assessed for two postcode areas of comparable size only (6701 ~ 2,1 km^2, 6705 ~ 2,4 km^2). These two postcode areas differ from high vegetation density (PC 6705) to low vegetation density (PC 6701).

Interestingly the difference of potential electricity yield gain of those two different areas is only 22,5%. This difference is caused by different household density.

Models which do not take the impact of tree shading into account (Hofierka & Kaňuk, 2009) lead to overestimation of the irradiation results. In the future optimal placement of PV can affect the tree planting planning.

6.6 Hot and cold spots

Since the only data available with regard to energy demand is yearly data, the match between energy production and demand may be inaccurate. Seasonal differences must be taken into account because of enormous difference in seasonal electricity production and in electricity demand. The supply in summer is higher than in the winter while the demand is lower in summer and higher in winter. Also calculated hot spots and cold spots do not take into account seasonal and daily demand and supply variations.

In theory the shared boundaries 4-digit postcode areas and 5-digit postcode areas should be equal, however since there is no official PostalCode-service the boundaries are changing over years. For that reason, results of hot spots/cold spots calculation may be slightly biased. Due to

use of both 4- digit postcode areas and 5- digit postcode areas from different years, hot spots and cold spots of postcodes 6701, 6702, 6703 are not accurate. This fact however does not affect the mismatch of whole Wageningen.

Some 5-digit postcodes stated in E-atlas do not exist since they usually represent large scale consumers. In addition, some buildings are intersected by postal codes boundaries, causing them to be listed twice in both 5 and 4-digit PCs.

Increasing share of locally produced renewable energy requires upgrades of old grid systems to a smart grid. Smart grid integrates generated electricity from small scale power sources (including solar and wind) along with utility companies. Due to two way communication infrastructure smart grid allows effective matching supply and demand. Smart grids are still in early development with challenges in the realization, also legislation and infrastructure has to be altered (European Commission, 2011; Moslehi & Kumar, 2010).

7 Conclusions and recommendations

This study on *estimation of electrical self-sufficiency in case of roof-top photovoltaic in the city of Wageningen by the analysis of LIDAR data shows* that the LIDAR can be a reliable base for estimation of height and orientation of buildings in Wageningen and determination of building outlines. However determination of building roofs requires time consuming manual supervision based on terrain knowledge. It is shown that 82% of LIDAR based footprints were detected well in comparison to BAG.

Zonatlas provides information regarding potential solar energy per building only. However to reach climate neutrality of Wageningen, the view from coarser/more global scale is also important.–This study demonstrates how spatial analysis can be employed to quantify energy hot spots and cold spots throughout Wageningen and its self-sufficiency. It was found out that PV electricity generation on all the available roof surface would cover the yearly electricity demand of Wageningen. Assuming only 75% of all roof surfaces are usable for PV installation, 2/3 of yearly consumption could be covered. However this does not cover seasonal and daily variations in demand (over day, over week and seasons) and supply (there is usually large surplus of load during summer and spring).

The fact that potential supply is higher than demand speaks in favor of energy storage, however demand and production in time are important aspects. In order to find out if energy storage is necessary or economically viable real-time management of electricity demand and supply needs to be evaluated. Options how to efficiently and effectively store the energy captured and make it available at the proper moment is being under research. Alternative market for unused electricity can be found - surplus energy from hot spots areas could be exported to cold spot areas.

Tree shading influences potential annual supply negatively. If vegetation influence was neglected, electricity yield would increase by 21% in less vegetated area (PC 6701) and by 43,5% in area with a lot of vegetation (PC 6705). Determination of the best roof configuration for energy conversion systems installations can be useful for further urban planning regarding the tree planting. It is quite possible that the solar energy development will lead to situations when there will be a need of legislation that recognizes access to sunlight as a right. For example: tree growing in your neighbor's property shading on your roof.
Further recommendations can be given in regard of future research. Opportunities to the future are limited by data and technologies available.

Future Data availability

Even though potential of individual roofs has been calculated, house owners should take into account condition of the building's roof. Since most of the solar panels have warranty up to 25 years and their life expectancy is even higher it is wise to predict possible roof rehabilitation necessities. It is recommended to install solar arrays either on almost new or recently rehabbed roofs so their life can be matched. For this reason data containing building´s renovation projects would be useful for matching solar panels acquisition with roof related renovation projects. I propose that municipalities or the authority responsible for renovation and new building approval should create the database based on data of the Netherlands cadaster.
Such a dataset already exists in the Netherlands. The municipality of Zaanstad is owner of dataset Woningbouwlocaties containing all planned, in progress and completed construction and renovation projects (Nationaal georegister, 2013).

Moreover in order to match the demand with supply most recent and detailed demand data is needed. Due to differences in energy demand over year, seasonal and longitudinal trend study of an electricity demand would be useful. Dutch privacy legislation prohibits providing any demand profiles or values for individual buildings for privacy reasons. Since these data are confidential, the asset companies cannot provide them widespread. These data might be implemented in related maps containing PV potential and CO_2 emissions savings and used for further decision support. Performance data of actual PV plants in Wageningen could be used for validation only in future.

Future research opportunities

Future research could focus on issues of roof shapes, area, patches and the role of south faced walls. Solar panels can be installed on nearly any roof. Compact shape roofs together with ideal orientation and moderate pitch provide higher solar potential. Possible research opportunity to future is to divide roofs according to their shapes and find optimal roof shape in terms of gaining maximum amount of solar energy by maximizing important to maximizing south facing roof areas and avoiding self-shading geometries. Optimal roof shapes in combination with suitable layout of street allow optimize PV potential.
Roof parameterization could be used for roofs reconstruction in case of missing LIDAR points (as mentioned in the discussion). Since the variety of roof types in Wageningen is very diverse, complex roofs can be modelled as a combination of basic geometry primitives. Modelling system working from LIDAR data and existing ground plans has to be implemented.
3D building reconstruction algorithm producing LOD2 models from ground plans and airborne LIDAR data was already developed in Germany and was used for cities of East Berlin and Cologne (Kada & McKinley, 2009). This method could be used in further studies.

The result of this thesis was focused on estimation of potential electricity yield and spatial distribution of energy hot spots and colds per urban regions in Wageningen. Due to its scale, the outcome of this thesis can be used for planning in order to meet the ambition of the municipality of Wageningen to climate neutral to be in 2030. The result is however no substitute for an on-site assessment by a PV installer. For an accurate calculation of potential electricity yield per building

and, small structures, such as dormers or chimneys must be eliminated. In order to be suitable for placement of solar panels only the most favorable homogenous roof faces in terms of solar radiation must be taken into account. To determine the actual usable roof surface, a refinement / further development of used method is needed.
Overview of individual roof patches – homogenous roof planes with certain area, tilt and orientation could be useful for studies regarding solar energy potential in smaller scale or green roofs and run-off of water studies.
CityGML 3D solar energy potential cadasters considering both roof and south-wall mounted systems can be created. It would be beneficial both time-saving wise and also accuracy wise. The Netherlands aims for the production of a large scale 3D geo-database but unfortunately 3D model of the Netherlands is currently in preparation phase (Stoter et al., 2013).
Spacemate (PERMETA Architects, 2001), describing the urban form of different neighborhoods with indicators like Floor Space Index and Gross Space Index could be integrated to this method.

References

Akbari, H., Kurn, D., Bretz, S., & Hanford, J. (1997). Peak power and cooling energy savings of shade trees. *Energy and Buildings*, *25*, 139–148. Retrieved from http://www.sciencedirect.com/science/article/pii/S0378778896010031

ASPRS. (2012). Retrieved from http://www.asprs.org/

Baigorria, G. a., Villegas, E. B., Trebejo, I., Carlos, J. F., & Quiroz, R. (2004). Atmospheric transmissivity: distribution and empirical estimation around the central Andes. *International Journal of Climatology*, *24*(9), 1121–1136. doi:10.1002/joc.1060

Bergamasco, L., & Asinari, P. (2011). Scalable methodology for the photovoltaic solar energy potential assessment based on available roof surface area: Application to Piedmont Region (Italy). *Solar Energy*, *85*(5), 1041–1055. doi:10.1016/j.solener.2011.02.022

Bortolini, M., Gamberi, M., Graziani, A., Mora, C., & Regattieri, A. (2013). Multi-parameter analysis for the technical and economic assessment of photovoltaic systems in the main European Union countries. *Energy Conversion and Management*, *74*, 117–128. doi:10.1016/j.enconman.2013.04.035

Bourget, L. (2013). *Solar Energy*. (C. Richter, D. Lincot, & C. A. Gueymard, Eds.) (pp. 226–687). New York, NY: Springer New York. doi:10.1007/978-1-4614-5806-7

Brito, M. C., Gomes, N., Santos, T., & Tenedório, J. A. (2012). Photovoltaic potential in a Lisbon suburb using LiDAR data. *Solar Energy*, *86*(1), 283–288. doi:10.1016/j.solener.2011.09.031

Burger, B., & Ruther, R. (2005). Site-dependent system performance and optimal inverter sizing of grid-connected PV systems. *Photovoltaic Specialists Conference, 2005. Conference Record of the Thirty-First IEEE*. doi:10.1109/PVSC.2005.1488469

Carneiro, C., Morello, E., & Desthieux, G. (2009). Assessment of Solar Irradiance on the Urban Fabric for the Production of Renewable Energy using LIDAR Data and Image Processing Techniques. In M. Sester, L. Bernard, & V. Paelke (Eds.), *Advances in GIScience SE - 5* (pp. 83–112). Springer Berlin Heidelberg. doi:10.1007/978-3-642-00318-9_5

Charabi, Y., & Gastli, A. (2013). Integration of temperature and dust effects in siting large PV power plant in hot arid area. *Renewable Energy*, *57*, 635–644. doi:10.1016/j.renene.2013.02.031

Climatemps. (2013). Retrieved July 04, 2013, from http://www.netherlands.climatemps.com/

Dash, J., Steinle, E., Singh, R. ., & Bähr, H. . (2004). Automatic building extraction from laser scanning data: an input tool for disaster management. *Advances in Space Research*, *33*(3), 317–322. doi:10.1016/S0273-1177(03)00482-4

EIA. (2013). *International Energy Outlook, 2013* (pp. 1–300). Washington, DC. Retrieved from http://books.google.com/books?hl=en&lr=&id=vebDRK0a6OAC&oi=fnd&pg=PA9&dq=International+Energy+Outlook+2013&ots=rzdSBsxeTS&sig=3e1V__niDa0T_-0PJSXxejKMFgk

El-Shobokshy, M., & Hussein, F. (1993). Effect of dust with different physical properties on the performance of photovoltaic cells. *Solar Energy*, *5*(6), 505–511. Retrieved from http://www.sciencedirect.com/science/article/pii/0038092X9390135B

Encyclopaedia Britannica. (2013). Relative humidity. In *Encyclopaedia Britannica Online*. Encyclopædia Britannica, Inc. Retrieved from http://www.britannica.com/EBchecked/topic/496857/relative-humidity

EREC. (2011). *Mapping Renewable Energy Pathways towards 2020* (pp. 4–104). Brussels.

ESRI. (n.d.-a). ArcGIS Help 10.1. *Area Solar Radiation*. Retrieved August 28, 2013, from http://resources.arcgis.com/en/help/main/10.1/index.html#//009z000000tm000000

ESRI. (n.d.-b). ArcGIS Help 10.1. *Classifying numerical fields for graduated symbology*. Retrieved December 01, 2013, from http://resources.arcgis.com/en/help/main/10.1/index.html#//00s50000001r000000

European Commission. (2011). European Technology Platform. *Strategic Deployment Document for Europe's Electricity*. Retrieved from http://scholar.google.com/scholar?hl=en&btnG=Search&q=intitle:European+Technology+Platform#5

Flood, M., & Gutelius, B. (1997). Commercial Implications of Topographic Terrain Mapping Using ScanningAirborne Laser Radar. *Photogrammetric Engineering and Remote Sensing*, *63*(4), 327–332. Retrieved from http://asprs.org/a/publications/pers/97journal/april/highlight.pdf

Fu, P., & Rich, P. (1999). Design and implementation of the Solar Analyst: an ArcView extension for modeling solar radiation at landscape scales. *Proceedings of the 19th Annual ESRI User Conference*. Retrieved from http://professorpaul.com/publications/fu_rich_1999_esri.pdf

Georgopoulos, A., & Tsakiri, M. (2004). Large scale orthophotography using DTM from terrestrial laser scanning. *The International Archives of the Photogrammetry, Remote Sensing and Spatial Information Sciences*, *XXXV*. Retrieved from http://218.196.194.5/portal/wenxian/gis article/599.pdf

Gross, M. (1997). Estimation of output enhancement of a partially shaded BIPV array by the use of AC modules. In *Photovoltaic Specialists Conference* (pp. 1381–1384). Conference Record of the Twenty-Sixth IEEE. doi:10.1109/PVSC.1997.654348

Gwandu, B., & Creasey, D. (1995). Humidity: a factor in the appropriate positioning of a photovoltaic power station. *Renewable Energy*.

Heslinga, M. W., Meijer, H., Rowen, H. H., & Wintle, M. J. (n.d.). Netherlands. In *Encyclopaedia Britannica Online*. Encyclopædia Britannica, Inc. Retrieved from http://www.britannica.com/EBchecked/topic/409956/Netherlands/35861/Climate

Highman, K. (2011). *An Analysis of Solar Rooftop Mapping Techniques & Outputs*. Bristol.

Hofierka, J., & Kaňuk, J. (2009). Assessment of photovoltaic potential in urban areas using open-source solar radiation tools. *Renewable Energy*, *34*(10), 2206–2214. doi:10.1016/j.renene.2009.02.021

Hussein, H. M. S., Ahmad, G. E., & El-Ghetany, H. H. (2004). Performance evaluation of photovoltaic modules at different tilt angles and orientations. *Energy Conversion and Management*, *45*(15-16), 2441–2452. doi:10.1016/j.enconman.2003.11.013

Ibrahim, A., Othman, M. Y., Ruslan, M. H., Mat, S., & Sopian, K. (2011). Recent advances in flat plate photovoltaic/thermal (PV/T) solar collectors. *Renewable and Sustainable Energy Reviews*, *15*(1), 352–365. doi:10.1016/j.rser.2010.09.024

IEA PVPS. (2002). *Potential for building integrated photovoltaics*. *IEA-PVPS Task* (Vol. 2002, pp. 1–12). Retrieved from www.iea-pvps.org

IEA PVPS. (2012). Trends in photovoltaic applications survey report of selected IEA countries between 1992 and 2011. Retrieved from www.iea-pvps.org

Jakubiec, J. A., & Reinhart, C. F. (2013). A method for predicting city-wide electricity gains from photovoltaic panels based on LiDAR and GIS data combined with hourly Daysim simulations. *Solar Energy*, *93*, 127–143. doi:10.1016/j.solener.2013.03.022

Jochem, A., Höfle, B., Hollaus, M., & Rutzinger, M. (2009). Object detection in airborne LIDAR data for improved solar radiation modeling in urban areas. *The International Archives of the Photogrammetry, Remote Sensing and Spatial Information Sciences*, *XXXVIII*(ii). Retrieved from http://wl27www658.webland.ch/bh/docs/papers/2009/Jochem_et_al_IAPRS_Paris_2009.pdf

Jochem, A., Höfle, B., Rutzinger, M., & Pfeifer, N. (2009). Automatic roof plane detection and analysis in airborne lidar point clouds for solar potential assessment. *Sensors (Basel, Switzerland)*, *9*(7), 5241–62. doi:10.3390/s90705241

Jochem, A., Höfle, B., Wichmann, V., Rutzinger, M., & Zipf, A. (2012). Area-wide roof plane segmentation in airborne LiDAR point clouds. *Computers, Environment and Urban Systems*, *36*(1), 54–64. doi:10.1016/j.compenvurbsys.2011.05.001

JRC. (2012). PVGIS. Retrieved from http://re.jrc.ec.europa.eu/pvgis/

Kada, M., & McKinley, L. (2009). 3D building reconstruction from LiDAR based on a cell decomposition approach. … *Archives of Photogrammetry, Remote Sensing and …*, *XXXVIII*, 3–4. Retrieved from http://citeseerx.ist.psu.edu/viewdoc/download?doi=10.1.1.177.2904&rep=rep1&type=pdf

Kadaster. (n.d.). Kadaster. Retrieved October 20, 2013, from http://www.kadaster.nl/web/english/Annual-report/Products-and-services/Acquisition-and-registration.htm

Kalogirou, S. (2003). The potential of solar industrial process heat applications. *Applied Energy*, *76*(4), 337–361. doi:10.1016/S0306-2619(02)00176-9

Kalogirou, S. a., Agathokleous, R., & Panayiotou, G. (2013). On-site PV characterization and the effect of soiling on their performance. *Energy*, *51*, 439–446. doi:10.1016/j.energy.2012.12.018

Kassner, R. (2008). Analysis of the solar potential of roofs by using official lidar data. … *Sensing and Spatial …*, 2–7. Retrieved from http://www.emmy-humboldt.09y11.de/PDF_Dateien/SE_3_Kassner_Bereth_2008.pdf

Kodysh, J. B., Omitaomu, O. a., Bhaduri, B. L., & Neish, B. S. (2013). Methodology for estimating solar potential on multiple building rooftops for photovoltaic systems. *Sustainable Cities and Society*, *8*, 31–41. doi:10.1016/j.scs.2013.01.002

Koehl, M., Heck, M., & Wiesmeier, S. (2012). Modelling of conditions for accelerated lifetime testing of Humidity impact on PV-modules based on monitoring of climatic data. *Solar Energy Materials and Solar Cells*, *99*, 282–291. doi:10.1016/j.solmat.2011.12.011

Kruza, M. (2011). *Green roofs : potential for energy production and saving*. Wageningen University.

Kumar, R., & Rosen, M. a. (2011). A critical review of photovoltaic–thermal solar collectors for air heating. *Applied Energy*, *88*(11), 3603–3614. doi:10.1016/j.apenergy.2011.04.044

Levinson, R., Akbari, H., Pomerantz, M., & Gupta, S. (2009). Solar access of residential rooftops in four California cities. *Solar Energy*, *83*(12), 2120–2135. doi:10.1016/j.solener.2009.07.016

Liander. (2010). *E-atlas*. Duiven. Retrieved from www.liander.nl

Ludwig, D., Lanig, S., & Klärle, Bm. (2009). Sun-Area Towards Location-Based Analysis for Solar Panels by High Resolution Remote Sensors (Lidar). In *The World's GeoSpatial Solutions*. Santiago, Chile: International Cartographic Association. Retrieved from http://training.esri.com/bibliography/index.cfm?event=general.RecordDetail&ID=129231

Lukač, N., Žlaus, D., Seme, S., Žalik, B., & Štumberger, G. (2012). Rating of roofs' surfaces regarding their solar potential and suitability for PV systems, based on LiDAR data. *Applied Energy*, *102*, 803–812. doi:10.1016/j.apenergy.2012.08.042

Mani, M., & Pillai, R. (2010). Impact of dust on solar photovoltaic (PV) performance: Research status, challenges and recommendations. *Renewable and Sustainable Energy Reviews*, *14*(9), 3124–3131. doi:10.1016/j.rser.2010.07.065

Masters, G. M. (2004). *Renewable and Efficient Electric Power Systems*. Hoboken, NJ, USA: John Wiley & Sons, Inc. doi:10.1002/0471668826

Mekhilef, S., Saidur, R., & Kamalisarvestani, M. (2012). Effect of dust, humidity and air velocity on efficiency of photovoltaic cells. *Renewable and Sustainable Energy Reviews*, *16*(5), 2920–2925. doi:10.1016/j.rser.2012.02.012

Mondol, J. D., Yohanis, Y. G., & Norton, B. (2006). Optimal sizing of array and inverter for grid-connected photovoltaic systems. *Solar Energy*, *80*(12), 1517–1539. doi:10.1016/j.solener.2006.01.006

Moslehi, K., & Kumar, R. (2010). A reliability perspective of the smart grid. *Smart Grid, IEEE Transactions on*, *1*(1), 57–64. Retrieved from http://ieeexplore.ieee.org/xpls/abs_all.jsp?arnumber=5467283

Nishioka, K., Hatayama, T., Uraoka, Y., Fuyuki, T., Hagihara, R., & Watanabe, M. (2003). Field-test analysis of PV system output characteristics focusing on module temperature. *Solar Energy Materials and Solar Cells*, *75*(3-4), 665–671. doi:10.1016/S0927-0248(02)00148-4

Norton, B., Eames, P. C., Mallick, T. K., Huang, M. J., McCormack, S. J., Mondol, J. D., & Yohanis, Y. G. (2011). Enhancing the performance of building integrated photovoltaics. *Solar Energy*, *85*(8), 1629–1664. doi:10.1016/j.solener.2009.10.004

Notton, G., Lazarov, V., & Stoyanov, L. (2010). Optimal sizing of a grid-connected PV system for various PV module technologies and inclinations, inverter efficiency characteristics and locations. *Renewable Energy*, *35*(2), 541–554. doi:10.1016/j.renene.2009.07.013

Orioli, A., & Di Gangi, A. (2013). Load mismatch of grid-connected photovoltaic systems: Review of the effects and analysis in an urban context. *Renewable and Sustainable Energy Reviews*, *21*, 13–28. doi:10.1016/j.rser.2012.12.035

Palz, W. (1983). *Photovoltaic Power for Europe: An Assessment Study* (2nd ed., p. 198). D. Reidel Pub. Co. for the Commission of the European Communities (Dordrecht, Holland and Boston, U.S.A. and Hingham, MA). Retrieved from http://goo.gl/84nTdQ

Palz, W. (2012). Photovoltaic solar energy, spearheading Germany's renewable energy policy: an example to others. *EPJ Photovoltaics*, *3*, 30901. doi:10.1051/epjpv/2012003

PERMETA Architects. (2001). Spacemate. Retrieved March 25, 2014, from http://www.permeta.nl/spacemate/home/1.html

Rijksdienst voor het Cultureel Erfgoed. (n.d.). Rijksmonumenten. Retrieved November 25, 2013, from http://oud.cultureelerfgoed.nl/Monumenten/Erfgoedoverzicht monumenten/Gegevensbestanden rijksmonumenten/Rijksmonumenten datasets

Rijkswaterstaat Bestuursstaf. (2013). Landsdekkend hoogtebestand van hoge klasse. Retrieved August 09, 2013, from http://www.rijkswaterstaat.nl/actueel/nieuws_en_persberichten/2013/juni2013/landsdekkend_hoogtebestand_van_hoge_klasse.aspx

Rottensteiner, F., Trinder, J., Clode, S., & Kubik, K. (2005). Automated delineation of roof planes from lidar data. In *Laser scanning 2005* (pp. 221–226). Retrieved from http://www.ipf.tuwien.ac.at/publications/fr_enschede_2005.pdf

Salameh, M. G. (2003). Can renewable and unconventional energy sources bridge the global energy gap in the 21st century? *Applied Energy*, *75*(1-2), 33–42. doi:10.1016/S0306-2619(03)00016-3

Santos, T., Gomes, N., Brito, M., & Freire, S. (2011). Solar Potential Analysis in Lisbon Using LiDAR Data. *Earsel.org*, 13–19. Retrieved from http://www.earsel.org/symposia/2011-symposium-Prague/Proceedings/PDF/Coastal Zones/3 ok25-a2393-Santos_et_al.pdf

Sarver, T., Al-Qaraghuli, A., & Kazmerski, L. L. (2013). A comprehensive review of the impact of dust on the use of solar energy: History, investigations, results, literature, and mitigation approaches. *Renewable and Sustainable Energy Reviews*, *22*, 698–733. doi:10.1016/j.rser.2012.12.065

Sawka, M., Millward, A. a., Mckay, J., & Sarkovich, M. (2013). Growing summer energy conservation through residential tree planting. *Landscape and Urban Planning*, *113*, 1–9. doi:10.1016/j.landurbplan.2013.01.006

Siemer, J., & Knoll, B. (2013). Still more than enough. *PHOTON International*, (February), 72.

Singh, G. K. (2013). Solar power generation by PV (photovoltaic) technology: A review. *Energy*, *53*, 1–13. doi:10.1016/j.energy.2013.02.057

Siraki, A. G., & Pillay, P. (2012). Study of optimum tilt angles for solar panels in different latitudes for urban applications. *Solar Energy*, *86*(6), 1920–1928. doi:10.1016/j.solener.2012.02.030

Song, W., & Haithcoat, T. L. (2005). Development of comprehensive accuracy assessment indexes for building footprint extraction. *Geoscience and Remote Sensing, IEEE Transactions on*. doi:10.1109/TGRS.2004.838418

Stichting Zonne-energie Wageningen. (2013). lincense for monuments. Retrieved November 26, 2013, from http://www.zonne-energie-wageningen.nl/heb-ik-een-vergunning-nodig-voor-het-installeren-van-een-zonnestroomsysteem-enof-zonnepanelen-op-mijn-dak

Šúri, M., Huld, T. a., Dunlop, E. D., & Ossenbrink, H. a. (2007). Potential of solar electricity generation in the European Union member states and candidate countries. *Solar Energy*, *81*(10), 1295–1305. doi:10.1016/j.solener.2006.12.007

Tanaka, H. (2011). Solar thermal collector augmented by flat plate booster reflector: Optimum inclination of collector and reflector. *Applied Energy*, *88*(4), 1395–1404. doi:10.1016/j.apenergy.2010.10.032

tetraeder.solar. (n.d.). Zonatlas. Retrieved October 22, 2013, from www.zonatlas.nl

Thomas, R., Britain, G., Fordham, M., & Architects, F. (1999). Photovoltaics in buildings: a design guide. Retrieved from http://scholar.google.com/scholar?hl=en&btnG=Search&q=intitle:Photovoltaics+in+buildings:+a+design+guide#1

Tooke, T. R., Coops, N. C., Voogt, J. a., & Meitner, M. J. (2011). Tree structure influences on rooftop-received solar radiation. *Landscape and Urban Planning*, *102*(2), 73–81. doi:10.1016/j.landurbplan.2011.03.011

Tsoutsos, T., Frantzeskaki, N., & Gekas, V. (2005). Environmental impacts from the solar energy technologies. *Energy Policy*, *33*(3), 289–296. doi:10.1016/S0301-4215(03)00241-6

Tyagi, V. V., Rahim, N. a. a., Rahim, N. a., & Selvaraj, J. a. /L. (2013). Progress in solar PV technology: Research and achievement. *Renewable and Sustainable Energy Reviews*, *20*, 443–461. doi:10.1016/j.rser.2012.09.028

Van den Dobbelsteen, A., & Stremke, S. (Eds.). (2013). *Sustainable energy landscapes; designing, planning, and development* (p. 528). Taylor & Francis Group.

Voegtle, T., Steinle, E., & Tovari, D. (2005). Airborne laserscanning data for determination of suitable areas for photovoltaics. *International Archives of the …*, 215–220. Retrieved from http://www.isprs.org/proceedings/XXXVI/3-W19/papers/215.pdf

WBGU. (2013). WBGU. Retrieved April 04, 2013, from http://www.wbgu.de/en/home/

Wehr, A., & Lohr, U. (1999). Airborne laser scanning—an introduction and overview. *ISPRS Journal of Photogrammetry and Remote Sensing*, *54*(2-3), 68–82. doi:10.1016/S0924-2716(99)00011-8

Wiginton, L. K., Nguyen, H. T., & Pearce, J. M. (2010). Quantifying rooftop solar photovoltaic potential for regional renewable energy policy. *Computers, Environment and Urban Systems*, *34*(4), 345–357. doi:10.1016/j.compenvurbsys.2010.01.001

Wikipedia. (2013a). DTM. In *Wikipedia*. Retrieved from https://upload.wikimedia.org/wikipedia/commons/thumb/2/2c/DTM_DSM.png/320px-DTM_DSM.png

Wikipedia. (2013b). Lijst van rijksmonumenten in Wageningen. In *Wikipedia*. Retrieved from http://nl.wikipedia.org/wiki/Lijst_van_rijksmonumenten_in_Wageningen

Wittmann, H., Bajons, P., Doneus, M., & Friesinger, H. (1997). Identification of roof areas suited for solar energy conversion systems. *Renewable Energy*, *11*(1), 25–36. doi:10.1016/S0960-1481(96)00116-4

WRC. (2013). Retrieved April 06, 2013, from http://www.pmodwrc.ch/).

WUR. (2003). Weather station Haarweg. Retrieved from http://www.met.wau.nl/haarwegdata/readme/index.html

Yu, B., Liu, H., Wu, J., Hu, Y., & Zhang, L. (2010). Automated derivation of urban building density information using airborne LiDAR data and object-based method. *Landscape and Urban Planning*, *98*(3-4), 210–219. doi:10.1016/j.landurbplan.2010.08.004

Zangvil, A., & Aviv, O. E. (1985). Time variation in solar radiation in the negev, israel and its possible relation to the el chichon volcanic dust cloud. *Journal of Climatology*, *5*(4), 363–367. doi:10.1002/joc.3370050403

Zon, N. van der. (2011). *Kwaliteitsdocument AHN-2*. Amersfoort. Retrieved from http://www.ahn.nl/

Appendix 1: Electricity consumption

5-coded postcode	Electricity consumption (kWh)
6701A	5.558.247
6701B	4.788.692
6701C	2.690.367
6701D	2.731.015
6701E	459.08
6701G	81.22
6701P	972.31
6702A	2.861.916
6702B	1.387.337
6702C	996.52
6702D	18.669.644
6702E	675.54
6702P	2.108.218
6703A	5.524.376
6703B	10.035.415
6703C	1.324.928
6703D	1.659.088
6703E	759.67
6703G	571.36
6703J	150.79
6703P	-
6704A	798.78
6704P	1.755.111
6705A	665.82
6705B	1.568.470
6705C	982.24
6705D	662.91
6705N	-
6706A	1.577.839
6706B	720.85
6706C	646.66
6706D	821.03
6706E	2.011.185
6706G	433.81
6706H	513.07
6706J	708.23
6706K	3.081.923
6707A	2.377.289
6707B	918.79

6707C	928.31
6707D	1.076.044
6707E	1.550.314
6707G	1.417.818
6707H	807.91
6707J	519.42
6708A	2.469.813
6708B	909.51
6708C	771.72
6708D	858.62
6708E	756.14
6708G	1.420.900
6708H	1.948.267
6708J	1.180.489
6708K	1.056.562
6708L	1.651.720
6708M	820.23
6708N	1.422.837
6708P	33.890.404
6708R	1.980.862
6708S	1.467.138
6708T	969.49
6709D	2.260.765
6709P	13.829.589
6709R	2.392.096
Totaal	19880.03

Appendix 2: Calculation of atmospheric parameters

Monthly Solar Irradiation

Wageningen 51°57'52"N 5°39'47"E

PVGIS Estimates of long-term monthly averages

Month	H_h	H_{opt}	H(90)	DNI	I_{opt}	D/G
Jan	689	1230	1310	994	68	0,68
Feb	1250	1890	1800	1430	60	0,64
Mar	2480	3260	2680	2400	49	0,58
Apr	4330	5020	3420	4180	36	0,48
May	5030	5150	2940	4070	22	0,51
Jun	5430	5290	2800	4130	15	0,52
Jul	4990	4940	2740	3430	17	0,57
Aug	4130	4500	2850	3340	30	0,53
Sep	3040	3760	2880	2700	43	0,57
Oct	1740	2560	2340	1970	57	0,58
Nov	842	1410	1440	1090	65	0,67
Dec	618	1070	1130	779	68	0,75
Year	2890	3350	2360	2550	37	0,55

Haarweg D/G				
2008	2009	2010	2011	2012
0,436299	0,376172	0,527656	0,347483	0,408764
0,440045	0,589898	0,613886	0,470139	0,47646
0,544952	0,501783	0,503726	0,131991	0,478999
0,513027	0,43435	0,376048	0,386212	0,549126
0,399491	0,436125	0,466449	0,413034	0,554484
0,4519	0,474552	0,377796	0,465804	2,527467
0,496431	0,434406	0,3819	0,244802	N/A
0,5135	0,413032	0,510604	0,519765	N/A
0,543636	0,506752	0,491648	0,463647	N/A
0,481173	0,491747	0,46672	0,407911	N/A
0,479286	0,515099	0,468243	0,421885	N/A
0,38673	0,446227	0,469449	0,378829	N/A

H_h: Irradiation on horizontal plane (Wh/m^2/day)
H_{opt}: Irradiation on optimally inclined plane (Wh/m^2/day)
H(90): Irradiation on plane at angle: 90deg. (Wh/m^2/day)
DNI: Direct normal irradiation (Wh/m^2/day)
I_{opt}: Optimal inclination (deg.)
D/G: Ratio of diffuse to global irradiation (-)

Diffuse proportion												
	Jan	**Feb**	**Mar**	**Apr**	**May**	**Jun**	**Jul**	**Aug**	**Sep**	**Oct**	**Nov**	**Dec**
PVGIS	**0,68**	**0,64**	**0,58**	**0,48**	**0,51**	**0,52**	**0,57**	**0,53**	**0,57**	**0,58**	**0,67**	**0,75**
2011 Haarweg	0,35	0,47	0,40	0,39	0,41	0,47	0,53	0,52	0,46	0,41	0,42	0,38
2010 Haarweg	0,53	0,61	0,50	0,38	0,47	0,38	0,38	0,51	0,49	0,47	0,47	0,47
2009 Haarweg	0,38	0,59	0,50	0,43	0,44	0,47	0,43	0,41	0,51	0,49	0,52	0,45
2008 Haarweg	0,44	0,44	0,54	0,51	0,40	0,45	0,50	0,51	0,54	0,48	0,48	0,39
Avg Haarweg	**0,42**	**0,53**	**0,49**	**0,43**	**0,43**	**0,44**	**0,46**	**0,49**	**0,50**	**0,46**	**0,47**	**0,42**

Clearness index												
	Jan	**Feb**	**Mar**	**Apr**	**May**	**Jun**	**Jul**	**Aug**	**Sep**	**Oct**	**Nov**	**Dec**
2008 Haarweg	0,243	0,398	0,360	0,457	0,509	0,449	0,416	0,405	0,426	0,397	0,264	0,303
2009 Haarweg	0,364	0,250	0,381	0,503	0,485	0,438	0,430	0,493	0,427	0,392	0,242	0,252
2010 Haarweg	0,311	0,254	0,421	0,545	0,421	0,542	0,519	0,397	0,399	0,409	0,273	0,285
2011 Haarweg	0,295	0,303	0,498	0,545	0,513	0,439	0,398	0,407	0,449	0,447	0,366	0,267
Avg Haarweg	**0,303**	**0,301**	**0,415**	**0,512**	**0,482**	**0,467**	**0,441**	**0,426**	**0,425**	**0,411**	**0,286**	**0,277**

Appendix 3: Energy hot spots and cold spots

Table 17: Energy hot spots and cold spots based on 5-digit postcodes

5-coded post-code	Electricity consumption (kWh)	El. yield SUM (kWh)	El. yield buildings (kWh)	Hotspot (+)/coldspot (-) (kWh)	Consumption coverage (%)
6701A	5 558 247	3 942 551	3 738 375	-1 819 872	67%
6701B	4 788 692	2 783 228	2 772 096	-2 016 596	58%
6701C	2 690 367	1 844 470	1 581 498	-1 108 869	59%
6701D	2 731 015	3 864 804	3 610 385	879 370	132%
6701E	459 077	612 357	529 331	70 254	115%
6701G	81 216	105 216	94 084	12 868	116%
6701P	972 306	255 571	191 473	-780 833	20%
6702A	2 861 916	4 725 831	4 725 831	1 863 915	165%
6702B	1 387 337	2 561 031	2 561 031	1 173 694	185%
6702C	996 518	1 543 236	1 543 236	546 718	155%
6702D	18 669 644	14 822 206	14 739 482	-3 930 162	79%
6702E	675 536	0	0	-	-
6702P	2 108 218	7 592 052	7 577 679	5 469 461	359%
6703A	5 524 376	2 594 732	2 539 633	-2 984 743	46%
6703B	10 035 415	3 082 883	2 958 078	-7 077 337	29%
6703C	1 324 928	1 953 870	1 708 005	383 077	129%
6703D	1 659 088	1 400 090	1 400 090	-258 998	84%
6703E	759 672	2 455 724	2 455 724	1 696 052	323%
6703G	571 362	2 079 273	2 079 273	1 507 911	364%
6703J	150 785	389 397	389 397	238 612	258%
6703P	-	150 267	150 267	-	-
6704A	798 783	2 860 870	2 860 870	2 062 087	358%

6704P	1 755 111	1 814 269	1 814 269	59 158	103%
6705A	665 820	1 910 365	1 910 365	1 244 545	287%
6705B	1 568 470	2 877 408	2 809 340	1 240 870	179%
6705C	982 243	1 887 436	1 887 436	905 193	192%
6705D	662 914	893 433	893 433	230 519	135%
6705N	-	0	0	-	-
6706A	1 577 839	3 244 411	3 240 411	1 662 572	205%
6706B	720 853	2 312 281	2 312 281	1 591 428	321%
6706C	646 662	1 511 833	1 511 833	865 171	234%
6706D	821 032	1 727 030	1 727 030	905 998	210%
6706E	2 011 185	2 128 709	2 128 709	117 524	106%
6706G	433 814	1 262 812	1 262 812	828 998	291%
6706H	513 068	368 964	368 964	-144 104	72%
6706J	708 233	2 185 001	2 185 001	1 476 768	309%
6706K	3 081 923	2 858 417	2 858 417	-223 506	93%
6707A	2 377 289	1 813 675	1 813 675	-563 614	76%
6707B	918 790	1 878 192	1 878 192	959 402	204%
6707C	928 313	2 148 103	2 148 103	1 219 790	231%
6707D	1 076 044	2 695 601	2 695 601	1 619 557	251%
6707E	1 550 314	3 566 240	3 566 240	2 015 926	230%
6707G	1 417 818	2 336 870	2 336 870	919 052	165%
6707H	807 908	6 349 131	6 349 131	5 541 223	786%
6707J	519 422	11 337 593	11 337 593	10 818 171	2183%
6708A	2 469 813	6 651 109	6 651 109	4 181 296	269%
6708B	909 514	1 811 455	1 811 455	901 941	199%
6708C	771 720	770 687	770 687	-1 033	100%
6708D	858 615	1 212 636	1 212 636	354 021	141%

6708E	756 138	1 486 540	1 486 540	730 402	197%
6708G	1 420 900	1 411 649	1 411 649	-9 251	99%
6708H	1 948 267	2 473 139	2 473 139	524 872	127%
6708J	1 180 489	2 746 317	2 746 317	1 565 828	233%
6708K	1 056 562	1 906 485	1 906 485	849 923	180%
6708L	1 651 720	6 842 299	6 842 299	5 190 579	414%
6708M	820 229	1 448 692	1 448 692	628 463	177%
6708N	1 422 837	2 704 020	2 704 020	1 281 183	190%
6708P	33 890 404	31 388 911	31 355 485	-2 534 919	93%
6708R	1 980 862	3 698 111	3 698 111	1 717 249	187%
6708S	1 467 138	2 983 739	2 983 739	1 516 601	203%
6708T	969 490	1 986 117	1 986 117	1 016 627	205%
6709D	2 260 765	1 844 679	1 844 679	-416 086	82%
6709P	13 829 589	14 589 847	14 589 847	760 258	105%
6709R	2 392 096	1 492 490	1 492 490	-899 606	62%

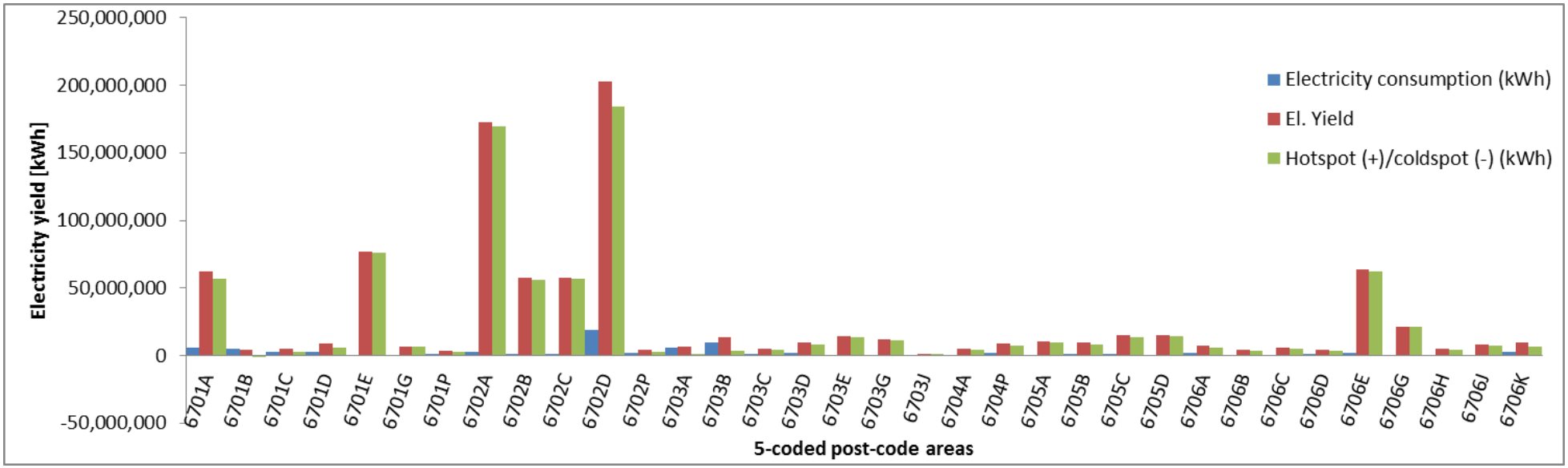

Figure 38: Energy hot spots and cold spots based on 5-digit postcodes (6701A-6706K)

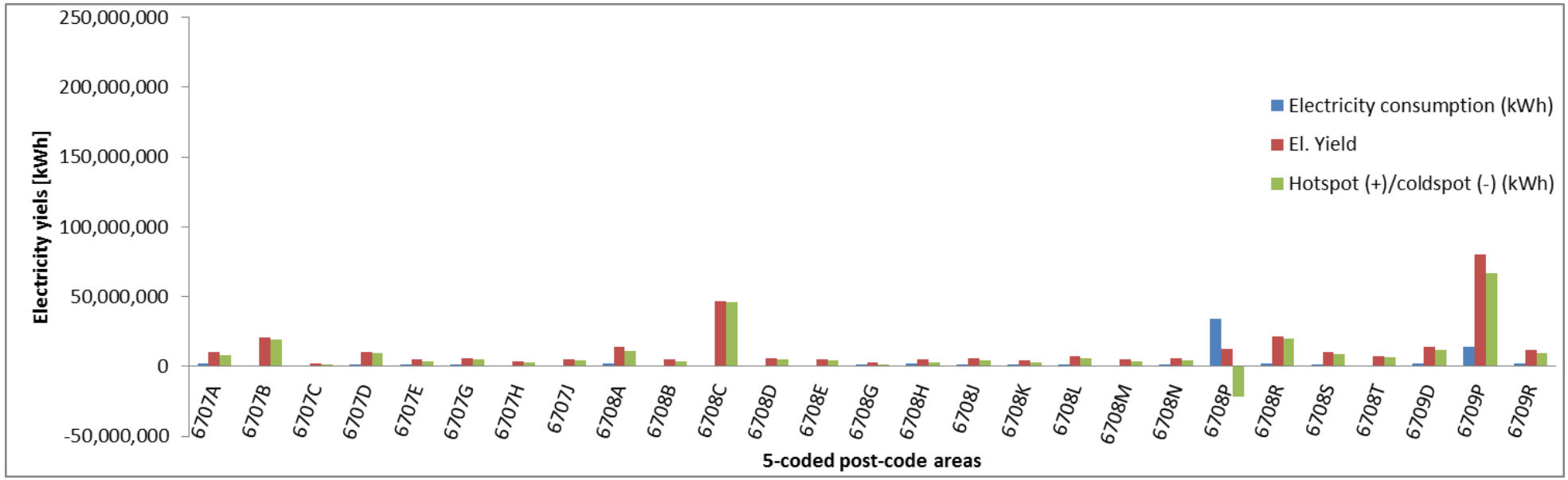

Figure 39: Energy hot spots and cold spots based on 5-digit postcodes (6707A-6709R)

Appendix 4: Validation

Table 18: Comparison of calculated electricity yield on gable roofs with Zonatlas values

Id	Area [m^2]	Electricity yield [kWh]	ZonatlasID	Zonatlas area [m^2]	Zonatlas yield [kWh]
1	817	106 944	962726	924	102 036
2	173	23 179	963727	198	22 907
3	18	2 245	939310	22	2 849
4	33	3 708	946734	36	4 246
5	24	3 149	947414	30	4 197
6	24	3 036	940322	31	3 779
7	28	3 645	939268	33	4 313
8	30	3 818	938243	33	4 273
9	33	4 260	958634	33	4 273
10	30	3 666	947799	43	5 127
11	71	9 644	939536	91	11 948
12	22	2 826	942376	32	4 295
13	23	3 169	950522	28	3 750
14	24	3 495	946773	26	3 454
15	23	3 194	946435	23	2 967
16	23	3 104	945803	32	4 150
17	22	2 906	951573	23	2 863
18	34	4 912	941497	32	4 236
19	20	2 772	949564	23	2 970
20	25	3 246	937311	27	3 421

Table 19: Comparison of calculated electricity yield on flat roofs with Zonatlas values

Id	Area [m2]	Electricity yield [kWh]	ZonatlasID	Zonatlas area [m2]	Zonatlas yield [kWh]
1	200	19 308	950500	188	7764
2	319	41 431	962626	298	12342
3	345	43 601	947446	359	37321
4	169	20 425	961839	149	6067
5	376	49 790	949468	344	14444
6	446	58 470	938576	433	17716
7	876	109 559	950444	849	33754
8	892	120 049	939218	810	34097
10	1 027	103 247	937198	920	39133
11	598	62 373	939444	586	24260
12	331	41 646	946535	346	14579
13	1 404	144 721	947468	1 273	54247
14	151	19 906	950516	148	15258
15	222	27 218	938164	216	9114
16	212	27 929	939263	213	8882
17	93	12 034	941788	95	3969
18	322	41 915	962626	298	12342
19	78	10 412	948813	78	3291
20	67	7 570	938639	66	2712
21	93	12 034	941788	95	3969
22	47	4 876	962798	46	1851
23	65	7 733	948415	64	2687